

# **Wireless Charging - some key elements**

Eva Palmberg, Sonja Lundmark, Mikael Alatalo, Torbjörn Thiringer  
and Robert Karlsson

*Department of Energy and Environment*

CHALMERS UNIVERSITY OF TECHNOLOGY

Göteborg, Sweden 2013



## Wireless Charging - some key elements

EVA PALMBERG, SONJA LUNDMARK, MIKAEL ALATALO, TORBJÖRN THIRINGER AND ROBERT KARLSSON

Department of Energy and Environment  
CHALMERS UNIVERSITY OF TECHNOLOGY  
Göteborg, Sweden 2013

## **Wireless Charging - some key elements**

Eva Palmberg, Sonja Lundmark, Mikael Alatalo, Torbjörn Thiringer and Robert Karlsson

Printed in Sweden Göteborg 2013

©Eva Palmberg, Sonja Lundmark, Mikael Alatalo, Torbjörn Thiringer and Robert Karlsson

Technical report 2013:1  
Department of Energy and Environment  
Division of Electric Power Engineering  
CHALMERS UNIVERSITY OF TECHNOLOGY  
SE-412 96 Göteborg  
Sweden

# Abstract

In this report so called wireless charging is investigated. The base concept investigated is a sending coil and a receiving coil at various heights, mainly using air, but also assisted with ferrites. Both analytical expressions as well as FEM analyses have been conducted. Regarding FEM analyses 2D as well as 3D analyses have been performed. Maxwell as well as Comsol Multiphysics have been utilised as FEM software.

The theory behind wireless energy transfer is presented and the dependencies of various geometrical parameters are established. The needed components for a wireless charging unit is described and analyzed, showing how design aspects (such as number of turns), frequencies, height and vertical displacement affect the results. Finally comparisons towards experiments have been done.

It is found that less sensitivity towards displacements can be achieved if the coils of the receiving coil are placed next to each other (instead of placing the coils as one inner ring coil inside an outer ring coil), and by increasing the air gap between a receiving and a sending coil. It is also shown that it is efficient to use ferrite plates adjacent to the coils in order to get more power to the load and to avoid high magnetic fields outside the charging system. It is also shown that coils (sending and/or receiving) with several conductors should have the outer conductor distanced from the inner ones as this will reduce skin effect, and therefore reduces the coil resistance.

The relatively long air gap of the wireless charging unit has some implications. There will be high leakage and a lot of flux will penetrate the winding, resulting in high losses at high frequencies. The thin conductors of a Litz-wire make it possible to lessen the eddy currents and skin effect in the conductors. It was further found that the efficiency of a 100 kW charging system was approximately 94 %.

Regarding comparisons between experiments and analytical expressions, it is found that the accuracy of the FEM model is especially important for the calculation of the resistance at high frequencies. The comparison between FEM programs and analytical calculations showed a small discrepancy. When comparing with measurements the discrepancy was larger. This could be explained with the complicated geometry of the coils.



# Acknowledgement

The authors would like to thank the 3rd year students at the school of Electrical Engineering 2010, 2011 and 2012 that have been constructing experimental equipment that has been used in this report.

Thanks also to Raquel Montalvo, who also conducted experiments that have been useful for this work.

The financial support given by Göteborg Energi AB is gratefully acknowledged.





# Contents

<b>Abstract</b>	<b>5</b>
<b>Acknowledgement</b>	<b>7</b>
<b>1 Introduction</b>	<b>11</b>
<b>2 Wireless transfer basics</b>	<b>13</b>
2.1 Geometry dependence of the mutual inductance $M$ at low frequencies, 2D . . .	13
2.1.1 Changing the geometry . . . . .	14
2.1.2 Geometry dependence of $M$ using ferrites . . . . .	18
2.1.3 Coupling factors . . . . .	23
2.1.4 Frequency dependence . . . . .	24
2.2 Calculation of the parameters in a cylindrical 3D model . . . . .	24
2.2.1 Current densities and losses in the wires . . . . .	26
2.2.2 Parameters . . . . .	27
2.2.3 Comparison of models . . . . .	27
2.3 Resonant coupling . . . . .	28
2.4 Conclusions of Chapter 2 . . . . .	29
<b>3 Modelling the wireless transfer coil system into Ansys</b>	<b>31</b>
3.1 Verification against analytical problems . . . . .	32
3.1.1 One long coil . . . . .	33
3.1.2 One ring coil . . . . .	34
3.1.3 Two ring coils . . . . .	35
3.2 Comparison to a master thesis work; two ring coils with Ferrite and Al-plates .	36
3.3 Comparison to a bachelor thesis work; a flat helix coil with 3 turns . . . . .	38
3.3.1 2D axisymmetric transient model of a flat circular coil with 3 turns . . .	39
3.3.2 A 3D transient model of a flat circular coil with 3 separate turns . . . .	41
3.3.3 A 3D transient model of a flat helix coil with 3 circular turns . . . . .	43
3.3.4 A 3D transient model of a flat helix coil with 3 rectangular turns . . . .	45
3.3.5 A 3D eddy current model of a flat helix coil, finer mesh . . . . .	47
3.3.6 Comparison to a bachelor thesis work; two frequencies . . . . .	47
3.4 Conclusions of Chapter 3 . . . . .	49
<b>4 Wireless charger unit</b>	<b>51</b>
4.1 Overview of charger . . . . .	51
4.2 Transformer . . . . .	52
4.3 Power Electronics . . . . .	58
4.4 Resonant circuit . . . . .	59
4.5 Control of transformer current . . . . .	60
4.6 Model and simulation results . . . . .	61
4.7 Alternative system . . . . .	64
4.8 Conclusions of Chapter 4 . . . . .	66
<b>5 Conclusions</b>	<b>67</b>



# Chapter 1

## Introduction

Today (2012) we are in the beginning of the installations of charger stations for electrified vehicles. So far the charging is made using 'conductive' techniques, i.e. that there is a direct electrical contact between charger and the vehicle, dominating is the concept of having a cable that is plugged in using some type of connector.

In order to make the charging more convenient, it would be very good if it could be more automated. Of course this can be done using the 'conductive technique', but more suitable would be to use the inductive principle where energy is transmitted from a sending coil to a receiving coil in the vehicles, so called 'inductive charging' or 'wireless charging'.

At the division of Electric Power Engineering at Chalmers University of Technology, a plug-in gokart is a subject of project for the students following the electrical engineering curriculum. In this, wireless charging is a theme where the students in projects do small steps in order to enhance the electrification in the plug-in gokart.

In order to develop this technique more knowledge about wireless charging is needed. Both fundamental theories as well as calculation methods needs to be enhanced and this has been made possible through the grant from Göteborg Energi that was awarded for this activity.

In order to summarize the wireless activities at the division of electric power engineering, this report has been written with the objective to

- Present the theory behind wireless energy transfer and establish the dependencies of various geometrical parameters.
- Compare various calculation complexities to establish the needs of deepness in the modelling.
- Describe the needed components for a wireless charging unit and for example determine the losses in the various parts.
- Determine how design aspects (such as number of turns), frequencies, height and vertical displacement affect the results.
- To verify some parts experimentally.



## Chapter 2

# Wireless transfer basics

## 2.1 Geometry dependence of the mutual inductance M at low frequencies, 2D

Let us study two rectangular loops in air, length 1 m in the z-direction, width 1 m each in the x-direction, see Figure 2.1. A current  $i_1$  flows in the lower (sending) loop. The induced voltage in the upper (pick-up) loop will be  $v_{ind_2} = M di_1 / dt$ . How will the mutual inductance  $M$  be changed when changing the geometry? The number of turns,  $N_1$  and  $N_2$ , the frequency and the currents in the loops will not be chosen yet.

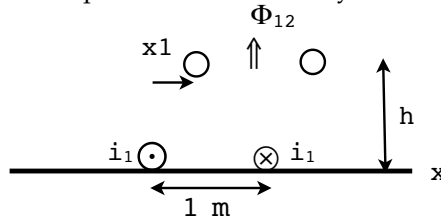


Figure 2.1: Two rectangular loops with current in the lower one. The upper loop is the pick-up loop. Unit length in the z-direction.

The flux through the pick-up loop is caused by the current  $i_1$  and  $M = N_2 \Phi_{12} / i_1$ . The flux can be written as  $\Phi_{12} = \int_S \mathbf{B}_{12} \cdot d\mathbf{s} = \oint \mathbf{A}_{12} \cdot d\mathbf{l}_2 = A_z(\text{left}) - A_z(\text{right})$ , where  $\mathbf{A}_{12}$  is the magnetic vector potential at the circumference of loop 2 caused by  $i_1$ . Maximum flux through loop 2, that is maximum  $M$ , will thus be for the difference in vector potentials being maximum. Or rather  $A_z(\text{left}) - A_z(\text{right})$  being maximal.

**a/ Analytical calculations** of the parameters for a loop, width  $d=1\text{m}$ , 1 m in the length direction, one turn and radius of the wire  $a=5 \cdot 10^{-3}\text{ m}$ , will give the self inductance  $L$ , as shown in equation 2.1.

$$L = \frac{\mu_0}{\pi} \left[ \frac{1}{4} + \ln \frac{d}{a} \right] \quad (2.1)$$

Dividing  $L$  into two parts  $L_{\text{outer}} = 2.11 \mu\text{H/m}$  and  $L_{\text{inner}} = 0.1 \mu\text{H/m}$ . -  $L_{\text{inner}} = \frac{\mu_0}{4\pi}$  is the inductance arisen from the magnetic fields inside the conductors. - For low frequencies  $L_{\text{tot}} = 2.21 \mu\text{H/m}$ . For very high frequencies  $L_{\text{inner}} = 0$ . The resistance  $R = 0.439 \text{ m}\Omega/\text{m}$  for low frequencies. When the frequency is chosen, we can calculate  $L_{\text{tot}}$  and the resistance  $R$ .

The calculation of the mutual inductance  $M$  will give the expression shown in equation 2.2 .

$$M = \frac{\mu_0}{2\pi} \ln \frac{r_2 r_3}{r_1 r_4} \quad (2.2)$$

where  $r_1 = \sqrt{h^2 + x_1^2}$ ,  $r_2 = \sqrt{h^2 + (x_1 + d_2)^2}$ ,  $r_3 = \sqrt{h^2 + (d_1 - x_1)^2}$  and  $r_4 = \sqrt{h^2 + (x_1 + d_2 - d_1)^2}$  Assuming two equal loops  $d_1 = d_2 = d = 1\text{ m}$ .

For  $x_1=0$  and  $h=0.1\text{ m}$  we get  $M = 0.92 \mu\text{H/m}$ . For  $x_1=0.1$  and  $h=0.1\text{ m}$  we get  $M = 0.78 \mu\text{H/m}$ .

**b/ A simulation** in Comsol's Multiphysics for  $i_1 = 1\text{A}$  in the sending loop will give the B-lines ( $A=\text{const}$ ) according to Figure 2.2. The reference for the vector potential  $A=0$  is set on the line  $x=0.5$ .  $A>0$  for  $x<0.5\text{ m}$  and  $A<0$  for  $x>0.5\text{ m}$ . **The pick-up loop must have one side to the left and the other side to the right so that  $A_z(\text{left}) - A_z(\text{right})$  will add for maximum  $M$ .** The vector potential is high close to the current loop.

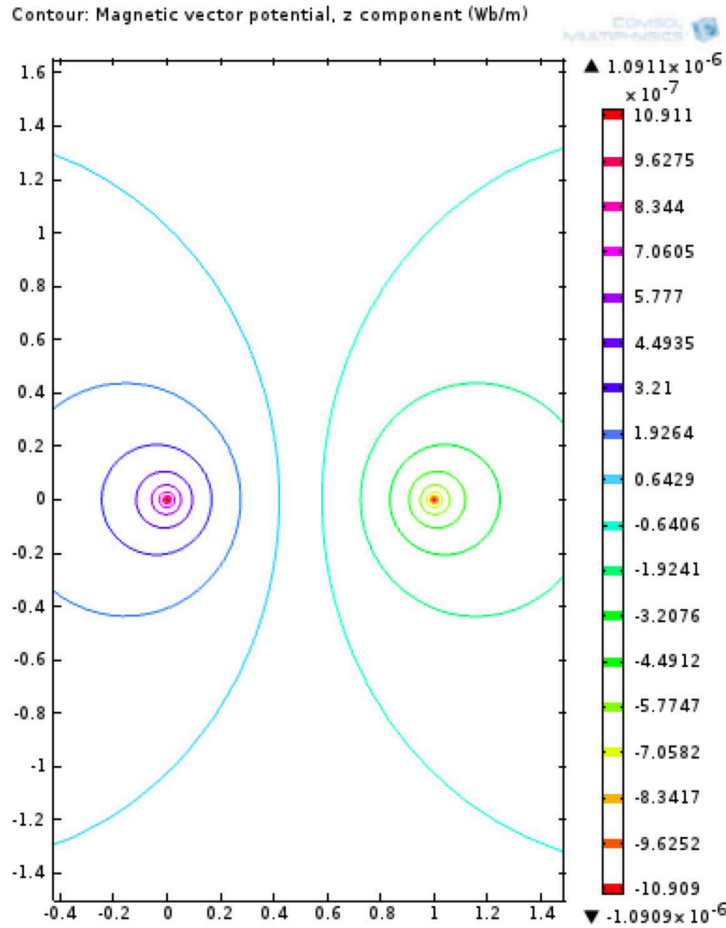


Figure 2.2: The B-lines ( $A=\text{const}$ ) from a rectangular loop with sides at  $x=0$  and  $x=1$  m. Current 1 A. Unit length in the  $z$ -direction. The colour legend shows the value of the vector potential on each line.  $A=0$  on the line  $x=0.5$  m

From the simulations we calculated the mutual inductance at the height  $h=0.1$  and the horizontal displacements  $x_1=0$  m and  $x_1=0.1$  m:  $M=0.92 \mu\text{H}/\text{m}$  respectively  $M = 0.78 \mu\text{H}/\text{m}$ . The same values as for the analytical calculation in section a/ above.

Let us now study the variation of  $A$  with the height above and distance to loop 1 in **air** in the next section. In later sections we introduce magnetic material close to the loops.

### 2.1.1 Changing the geometry

**Vertical displacements** of the pick-up loop: Figure 2.3 shows the vector potential  $A_z$  at different coordinates  $x$  and at different heights above loop 1.  $A_z=0$  in the middle of the loop ( $x=0.5$  m). The flux through loop 2 will be maximum if the width of the two loops are the same. Then the two  $A_z$ -values add:

$A_{z\text{max}} - (-A_{z\text{max}}) = 2A_{z\text{max}} = \Phi_{12}$ . The secondary loop must be placed at  $x=0$  and  $x=1$  m and at low height above loop 1 for maximum flux  $\Phi_{12}$ .

Changing the distance between the two loops from 5 cm to 10 cm will lessen the maximum possible  $M$  with 24% and the maximum possible power to a load with 42%!

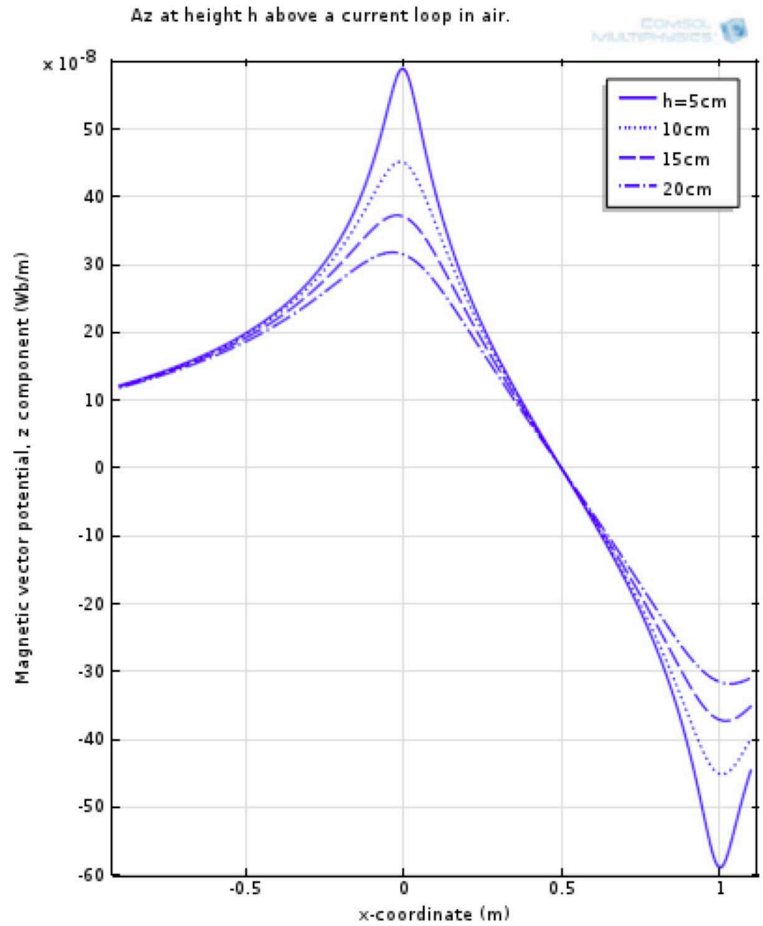


Figure 2.3: The vector potential  $A_z$  at height 5-25 cm above a current carrying loop between  $x=0$  and 1 m.

A **horizontal displacement**  $x_1$  of the upper loop will give a smaller  $M$ , see Figure 2.4! The order of magnitude of  $M$  is  $\mu\text{H}$ . A displacement of 5 cm at  $h=5\text{ cm}$  will give 11% lower  $M$ , while the same displacement at  $h=10\text{ cm}$  give 5% lower  $M$ . The higher height the less sensitivity to displacements, but the maximum  $M$  will also decrease with the height.

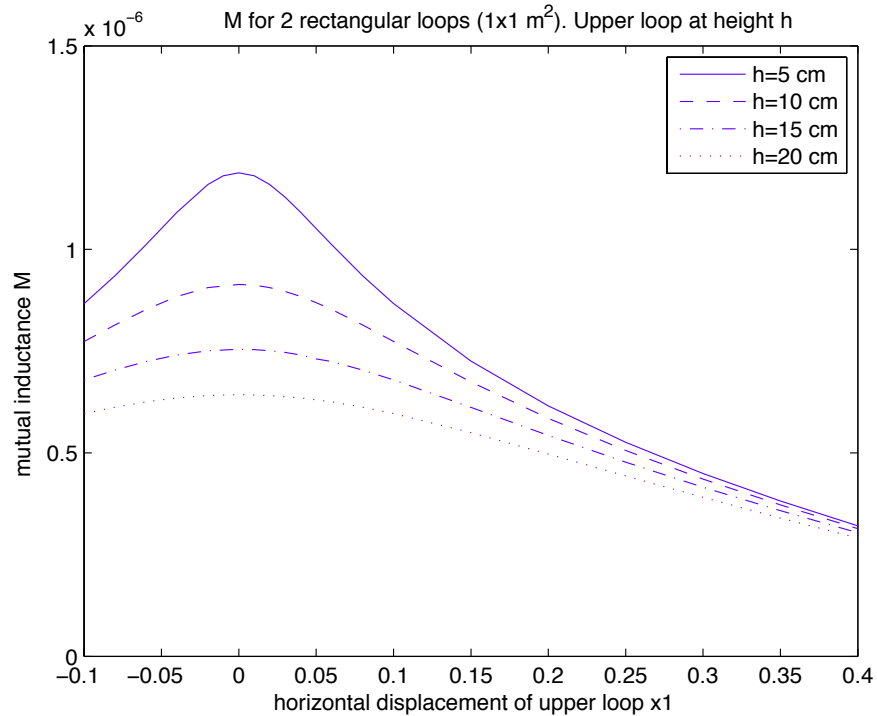


Figure 2.4: The mutual inductance between two rectangular loops, length 1 m, width 1m. The upper one displaced  $x_1$  horizontally from the lower one.

Can we design the magnetic field to be less sensitive to displacements of the secondary loop from the ideal position  $x_1=0$ ? Let us try in three different ways:

1. Use **another turn** at a small height  $h_{12}$  above the first turn in the **primary loop**. The geometry is shown in Figure 2.5.  $A_z$  for varying  $h_{12}$  is shown in Figure 2.6.

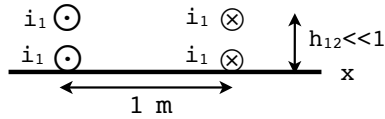


Figure 2.5: The 2 turns with 1A in each in the primary loop. The upper turn displaced  $h_{12}$  vertically from the lower one.

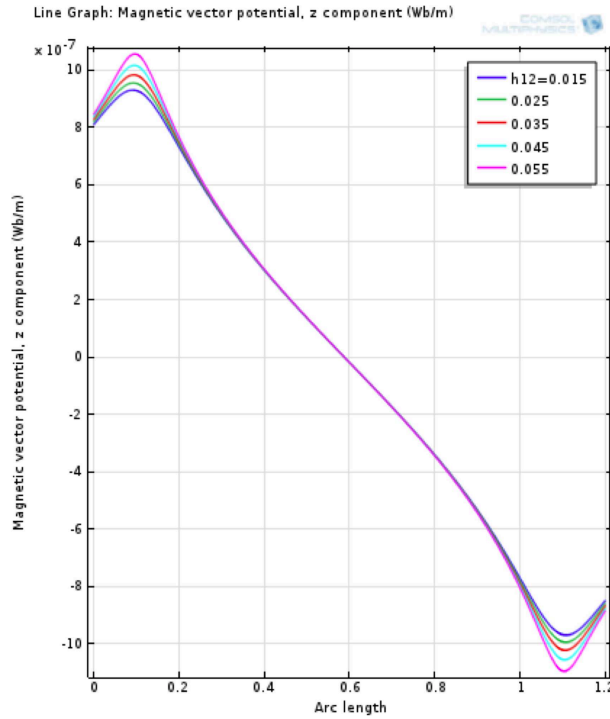


Figure 2.6: The vector potential at 10 cm above 2 turns, 1 A in each, in the primary loop, length 1 m, width 1 m. The upper turn is displaced  $h_{12}$  vertically from the lower one.

One extra turn **above** the first turn in the primary loop will only give a **lower  $A_z$ -values** close to the maximum of  $A_z$  than in the case of two loops in the same plane, see case 2 below!



2. Try instead a second turn be in the **same plane** as the first one. The geometry is shown in figure 2.7. Simulations for the vector potential in figure 2.8

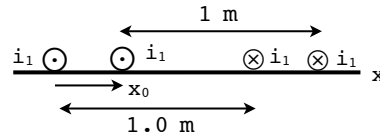


Figure 2.7: The 2 turns, width 1 m, length 1m with 1A in each. The second turn displaced  $x_0$  horizontally from the first one.

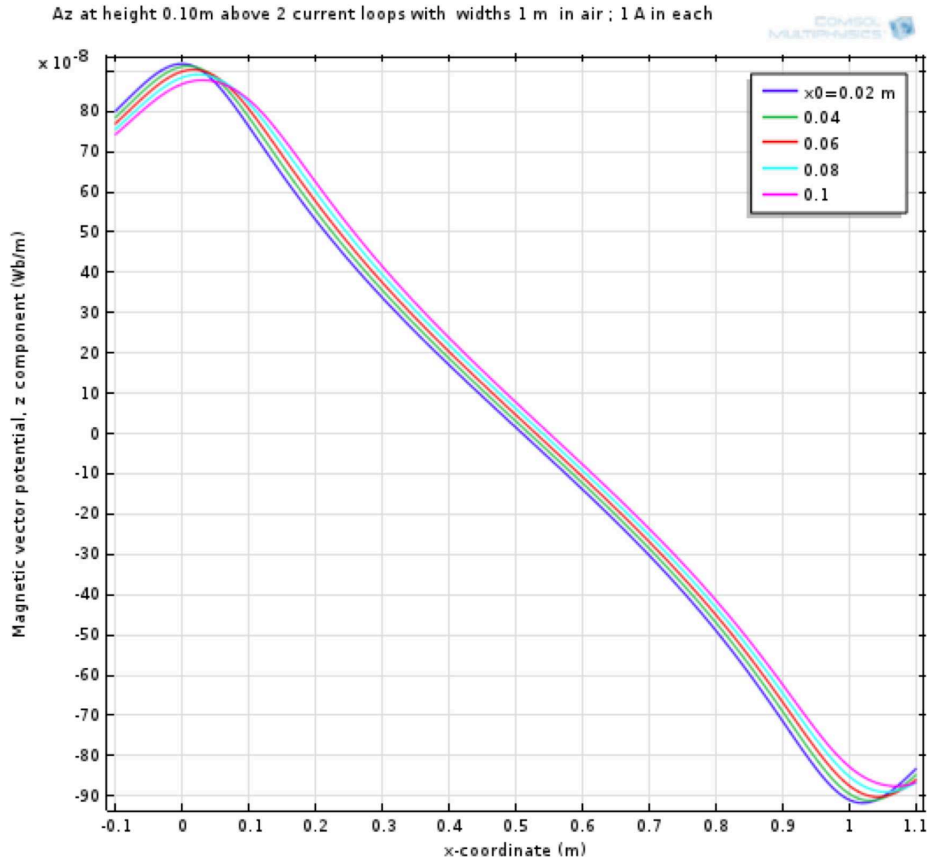


Figure 2.8: The vector potential at 10 cm above two turns in the primary loop, width 1 m both. The right one is displaced  $x_0$  horizontally from the left one.

Two turns displaced 2 cm from each other will just double  $A_{\max}$ , but the curve is rather steep. Using 5-10 cm displacement will give a  $A_z$  not so sensitive to horizontal displacements of the pick-up coil. (A horizontal displacement of the pickup coil with 5 cm will give -3 % in  $A_z$  ( $\sim M$ ). We can also see that  $k_{\text{new}}$  will show small variations (0.43 to 0.41), when the second turn is displaced horizontally from 2 cm to 10 cm.  $k_{\text{new}}$  is an interesting measure introduced later, section 2.1.3.)

**3. Smaller turns inside:** More smaller turns inside a bigger loop will not give so much higher higher  $A_z$  or  $M$ . Figure 2.9 shows a large loop width 1 m with a smaller loop, width 0.5 m inside. This will not give so high  $A_z$  (or  $M$ ) if we want only one turn in the pick-up loop. The highest  $A=67 \cdot 10^{-8}$  is lower than the highest  $A$  having two turns with almost equal width in the sending loop. We can also use the measure  $k_{\text{new}} = 0.32$ , a bad value!  $k_{\text{new}}$  will be introduced in section 2.1.3. The values are calculated here as an interesting measure.

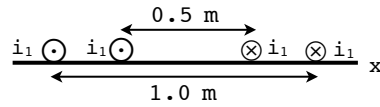


Figure 2.9: The 2 turns, widths 1.0 m and 0.5 m, length 1 m with 1 A in each.

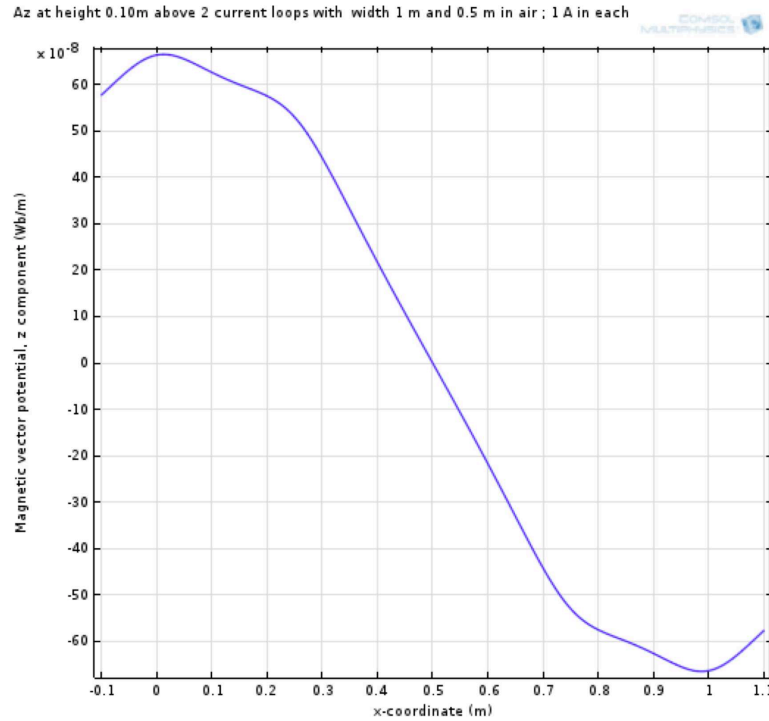


Figure 2.10: A from 2 loops width 1 m and 0.5 m. 1 A in each

**Result:** The second method placing the turns close to each other at the same height will be the best one. But some distance between the turns will give lower skin effect in the windings, see later!

### 2.1.2 Geometry dependence of M using ferrites

By using ferrite material we can get a better field image and higher mutual inductance  $M$ . A ferrite has high permeability and low conductivity.  $\sigma=1 \text{ S/m}$ ,  $\mu_r=1000$  are used here.

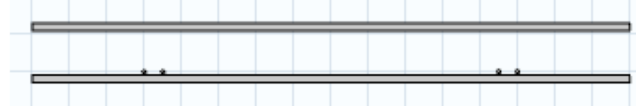


Figure 2.11: Two ferrite plates, drawn 0.3 m extra outside the two current loops. The distance between the plates is 0.11 m. The width of the loops are 1 m and 0.9 m, displaced 5 cm from each other in this figure.

#### Comparing the vector potential in three cases:

1.  $A_z$  at 10 cm above the two current loops,  $1 \times 1 \text{ m}^2$ , in air
2. The same as case 1 but including 2 ferrite sheets with width 1.25 m (10 cm outside the loops).
3. The same as case 2, but width of the ferrites is 2.25 m (60 cm outside the loops).

## The vector potential at 10 cm above the current loops

### Case 1, air

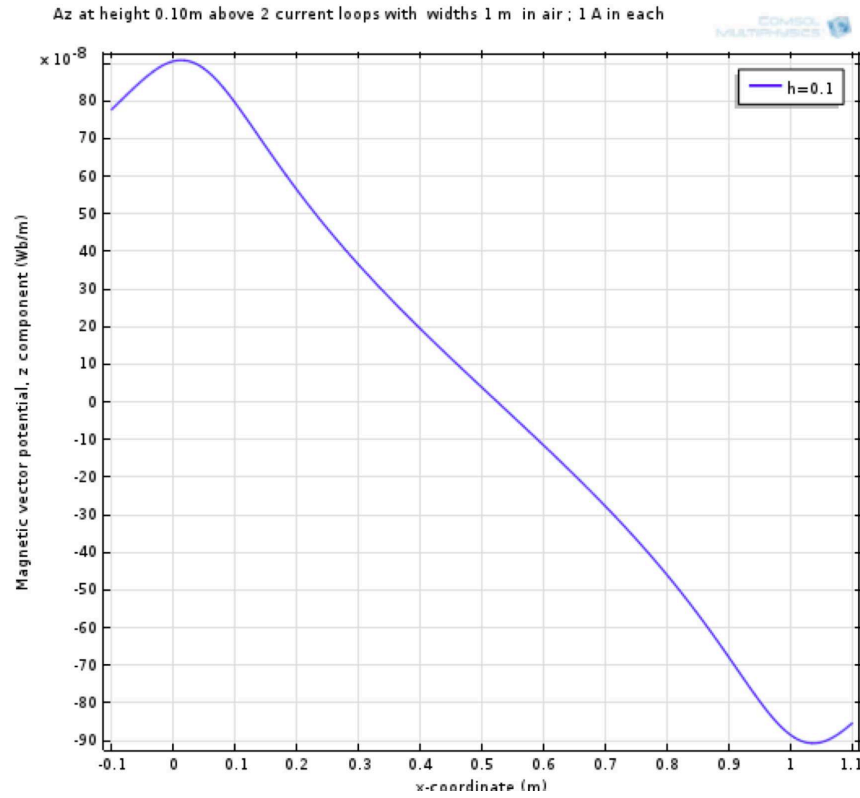


Figure 2.12: The vector potential at height 10 cm above two current loops in air. The width of the loops are 1 m each, displaced 5 cm from each other.

### Case 2, small ferrite plates:

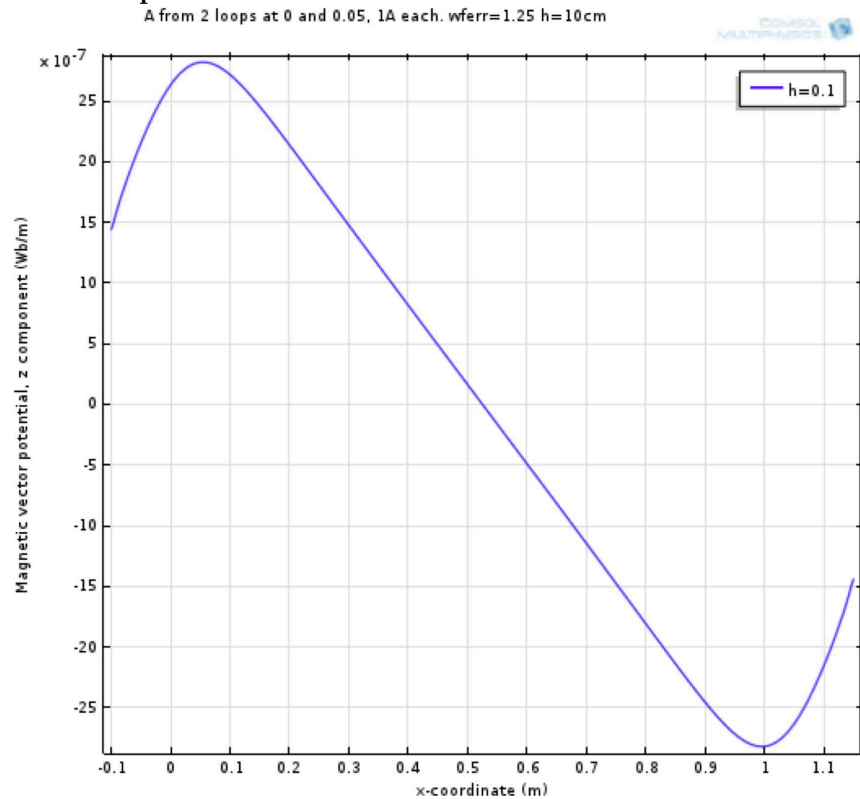


Figure 2.13:  $A_z$  at 10 cm above the two current loops. Two ferrite plates, drawn 0.1 m extra outside the two current loops. The distance between the plates is 0.11 m

### Case 3, bigger ferrite plates

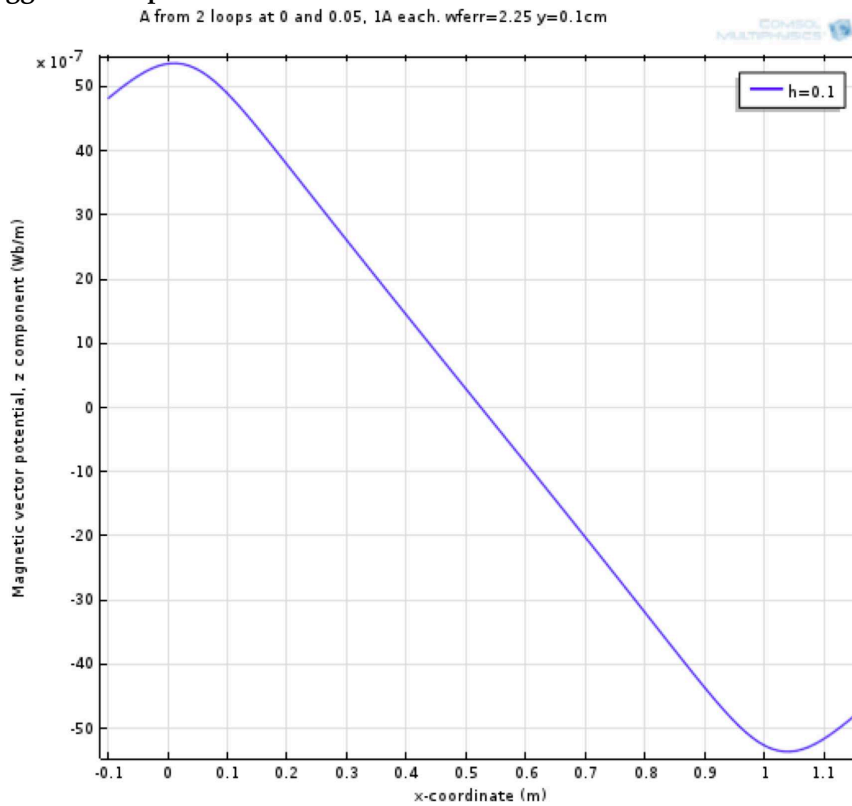


Figure 2.14:  $A_z$  at 10 cm above the two current loops. Two ferrite plates, drawn 0.6 m extra outside the two current loops. The distance between the plates is 0.11 m

From the three figures above we get the maximum vector potential  $A_{\max, \text{air}} = 9.1 \cdot 10^{-7}$  T;  $A_{\max, 1.25 \text{ ferrite}} = 28 \cdot 10^{-7}$  T;  $A_{\max, 2.25 \text{ ferrite}} = 54 \cdot 10^{-7}$  T; The biggest ferrite plates will give 5.9 times higher A (or mutual inductance M) than in air.

### The B-fields between and outside the ferrite plates

Case 2, small ferrite plates; only the left half of the field image shown:

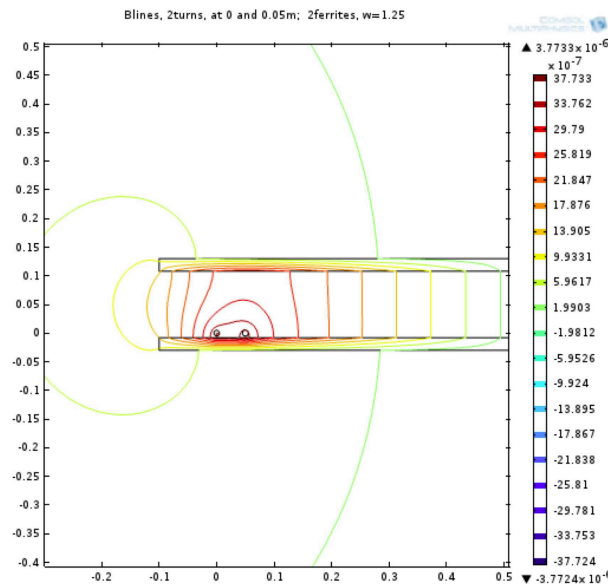


Figure 2.15: The field lines between the two ferrite plates, drawn 0.1 m outside the two current loops. The centre of the plates at  $x=0.5$  m.

### Case 3, bigger ferrite plates; only the left half of the field image shown

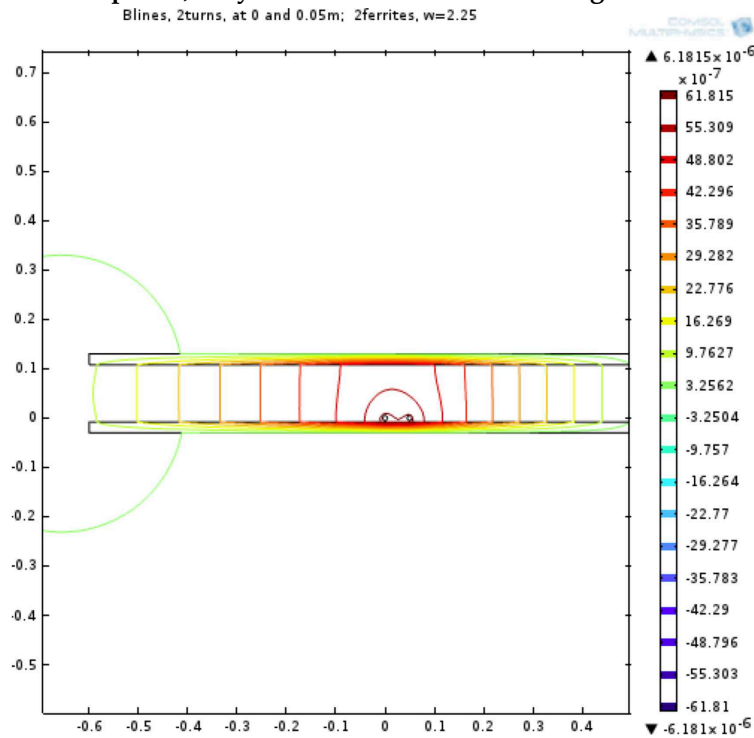


Figure 2.16: The field lines between the two ferrite plates, drawn out 0.6 m outside the two current loops. The centre of the plates at  $x=0.5$  m

**Result:** From the field images we can see that short ferrite plates (drawn out 10 cm outside the windings) will give a high magnetic field close to the windings. This can give skin effect in the wires. We also get high magnetic field outside the geometry. More than 10 cm extra ferrite will be necessary with all other parameters unchanged.

### The magnitude of the B-field – leakage flux

It is also interesting to look for the maximal value of the B-field in space. It will occur just outside the ends of the ferrite plates. Or more exact outside the upper face of the lower ferrite plate (lower face of the upper ferrite plate). The magnitude of the B-field is plotted on a vertical line drawn 5 mm outside the ends of the screens, see figure 2.17. In the Figures 2.18 and 2.19 the coordinate  $y$  is on the vertical and  $B$  on the **horizontal axis**.

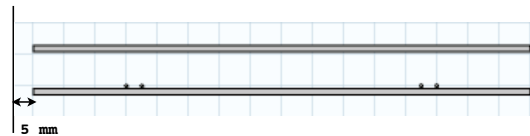


Figure 2.17: The ferrite planes and the windings. A vertical line is drawn 5 mm outside the plates. The B-fields on this line are shown in the next two figures.

### Case 2, small ferrite plates:

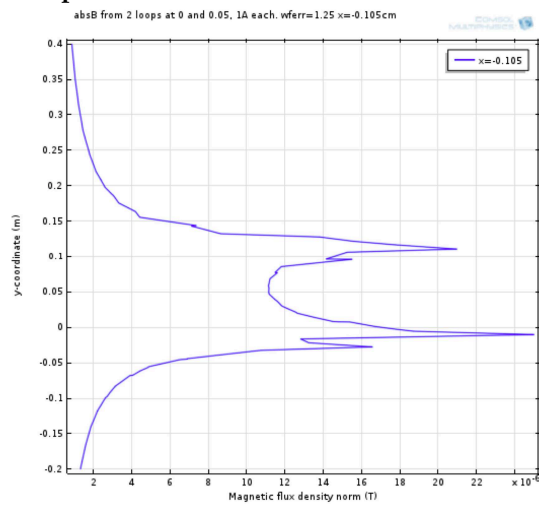


Figure 2.18: The magnitude of B on a vertical line 5 mm to the left of the ends of the ferrite plates, width 1.25 m.  $B_{\max}=25\mu\text{T}$

### Case 3, bigger ferrite plates

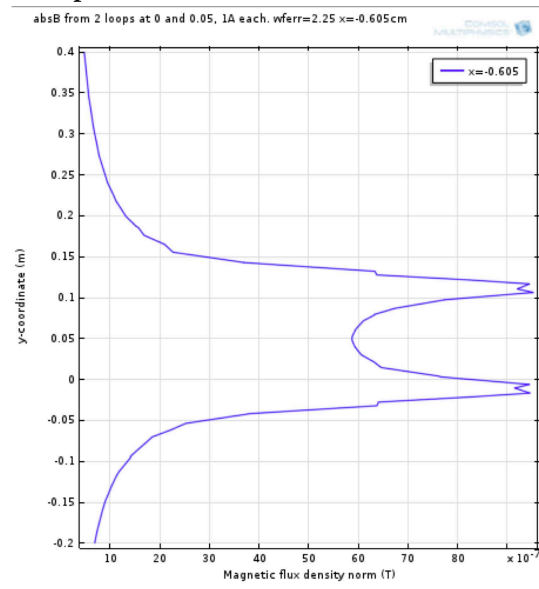


Figure 2.19: The magnitude of B on a vertical line 5 mm to the left of the ends of the ferrite plates, width 2.25 m.  $B_{\max}=9.5\mu\text{T}$

The peak values of B just outside the ferrite plates are  $25.0\mu\text{T}$  for 1.25 m ferrite and  $9.5\mu\text{T}$  for 2.25 m ferrite. Adding 50 cm extra on each side to the width of the ferrite will lessen the magnitude of B with 62 %! There are restrictions on the maximal B to be considered later.

How to get the best solution? Let us use a new coupling factor  $k_{\text{new}}$ !

### 2.1.3 Coupling factors

When using magnetically coupled circuits we usually use the coupling factor defined as

$$k = \frac{M}{\sqrt{L_1 L_2}} \quad (2.3)$$

(independent of the number of turns). For our case another coefficient will be useful, see equation 2.4!

$$k_{\text{new}} = \frac{N_2}{N_1} \frac{M}{L_2} \quad (2.4)$$

This expression is independent of the number of turns. It will only show the influence from the geometry and material.  $k_{\text{new}}$  is proportional to the maximum current that can be obtained in the pick-up circuit.  $k_{\text{new}}^2$  is proportional to the maximal power to the load. See section 2.3, equation 2.5!

Simplifying the simulations this calculation of  $k_{\text{new}}^2$  is done for two rectangular loops  $1 \times 1 \text{ m}^2$ . Each loop has a ferrite plate close to it. The values of  $k_{\text{new}}$  is shown in Table 2.1 for different materials, widths and distances between the two loops.

Table 2.1: Two  $1 \text{ m}^2$  rectangular current loops: coupling factor  $k_{\text{new}}$  for air or air + ferrite plates

material	vertical distance between loops	$k_{\text{new}} = N_2 M / (N_1 L_2)$
<b>air</b>	5 cm	0.56
	10 cm	0.43
	15 cm	0.36
	20 cm	0.30
<b>ferrite:</b> 1.2 m wide	5 cm	0.78
	10 cm	0.62
	15 cm	0.50
	20 cm	0.41
1.6 m wide	5 cm	0.85
	10 cm	0.71
	15 cm	0.51
	20 cm	0.50
2.2 m wide	5 cm	0.88
	10 cm	0.76
	15 cm	0.65
	20 cm	0.57

Coupling factors  $k_{\text{new}}$  around 0.4 or less are very bad. 0.9 will be a high coupling factor. For an ideal transformer  $k_{\text{new}} = 1$ .

#### Results from the table

Loops in air are not so useful, if the two loops cannot be closer than 5 cm. Ferrite plates will improve  $k_{\text{new}}$  and thus the maximum possible current in the secondary loop. 1.2 m wide plates will then double the power to the load. 2.2 m ferrite plates will give 3 times the power compared to two loops in air, 10 cm from each other!

Changing the distance between the two loops from 5 cm to 10 cm will lessen the maximum possible  $M$  with 24% and the maximum possible power to a load with 42% for air. Using big ferrite plates the same change in distance will lessen the maximum possible power to a load with 25%!

### 2.1.4 Frequency dependence

The simulations above are done for a wire radius of 5 mm and at low frequencies. Choosing a frequency of 20 kHz we must look at the skin depth in the copper windings.

$\delta_{20k} = 4.67 \cdot 10^{-4}$  m. We could use the radius of the wires  $a = 5 \cdot 10^{-4}$  m. We also want to send high currents so the wires must be in parallel in order to avoid too high current densities and also lessen the skin effect in the wires.

For a 3D design in the next section we will instead use flat wires,  $5\text{mm} \times 0.2\text{mm}$ . See calculations later.

Using the power loss in the wires for definition of R and the vector potential for calculation of L and M we can use the Comsol's Multiphysics Magnetic Field(mf) or Magnetic and Electric Field (mef) applications, or the Maxwell program. (Errors in the built-in calculations of the circuit parameters R, L and M still exist in both the programs, versions 4.3 and 15.0 respectively. These parameters cannot be used in our case.)

It is difficult to use the model of many parallel wires in the windings in a 3D simulation because of the different length scales of windings and volumes for the magnetic field calculations. We will make some simplifications, see next section!

## 2.2 Calculation of the parameters in a cylindrical 3D model

3D simulations of a geometry with big scale (loops and ferrite planes) and at the same time small scale (windings) are difficult. Let us make some modifications so we can use **symmetry** in the problem by using circular cylindrical geometry!

The **windings** are modelled as thin cylinders with radius of about 0.56 m at  $z=0$ , height 5 mm and thickness 0.2 mm. 15 isolated layers are coupled in parallel to make one turn. The area of this turn is about  $1 \text{ m}^2$ . The primary winding consists of 2 turn. The secondary winding with one turn is placed 10 cm above the primary one at radius  $r=0.54$  at  $z=0.1$ . The windings are just seen as black spots in the figure below.

Two ferrite planes, radius 0.816 m (extended 25 cm outside the windings), thickness 1.5 cm are placed 1 cm below the primary and above the secondary windings, see figure 2.20! The material constants used are  $\sigma_{\text{Cu}} = 5.8 \cdot 10^7 \text{ S/m}$ ,  $\sigma_{\text{ferrite}} = 1 \text{ S/m}$ ;  $\mu_{\text{rel,ferr}} = 1000$ ;

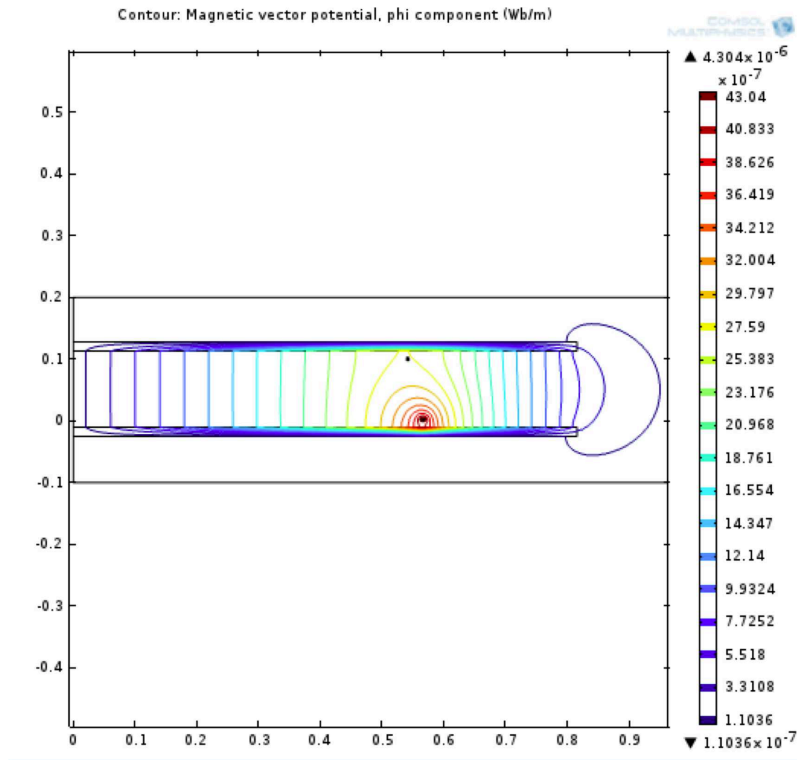


Figure 2.20: The geometry and the B-lines,  $A_\phi = \text{const}$  is the same as a B-line. The vertical axis,  $z$ , is the axis of symmetry. The horizontal axis is the radius  $r$ . Two turns in the primary winding are fed with 1A.



Figure 2.21 shows the mutual inductance  $M = A\phi \times 2\pi r$  as a function of the radius at the height  $z$ , where the secondary loop will be placed. The maximum  $M_{\max}$  will be at  $r=0.57$  m, so we ought to use that position for the secondary loop to get as high induced voltage as possible. Figure 2.22 shows the  $B_z$ -field at the same height.

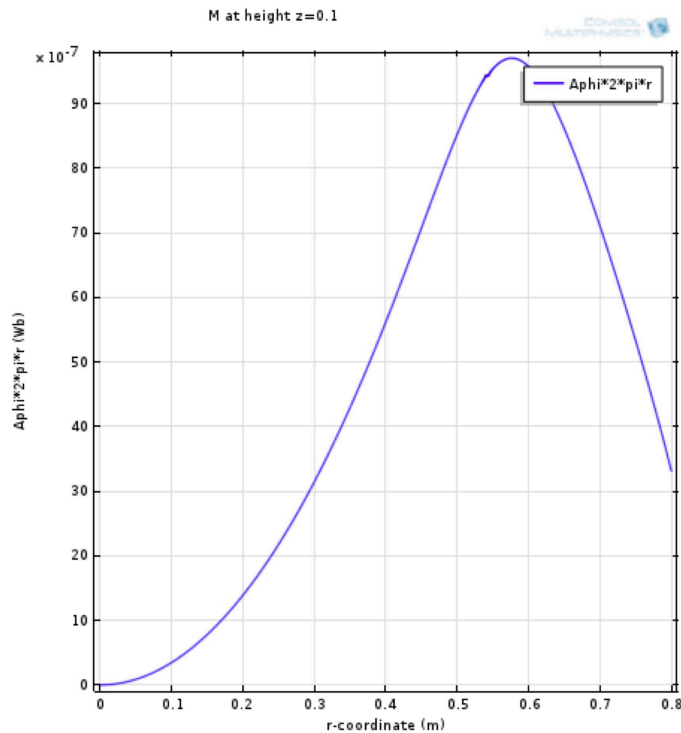


Figure 2.21: The mutual inductance  $M$  at height 0.1, when the two turns in the primary winding is fed with 1 A.  $M_{\max} = 9.69 \cdot 10^{-6}$  H at  $r=0.57$ .

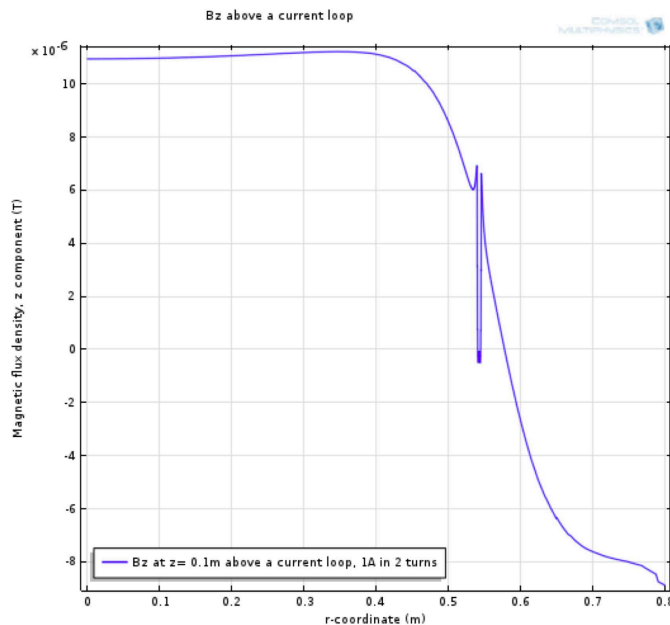


Figure 2.22: The magnetic field  $B_z$  at height 0.1, when two turns in the primary winding is fed with 1 A.  $B$  varies a lot just above the winding

Figure 2.23 shows the magnetic field on a line 10 cm outside the ferrite plates.

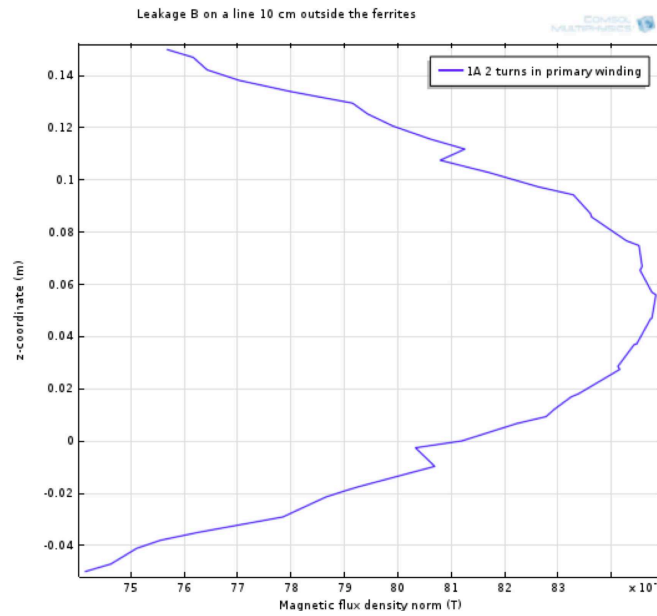


Figure 2.23: The leakage flux on a vertical line 10 cm outside the ferrite plates.  $B_{\max}=0.85 \mu\text{T}$

### 2.2.1 Current densities and losses in the wires

The wires are made thin and flat so that the skin effect will be lowered. Figure 2.24 shows the current density in the primary winding for 1 A in the two turns and figure 2.25 the current density in the secondary one also for 1 A secondary.

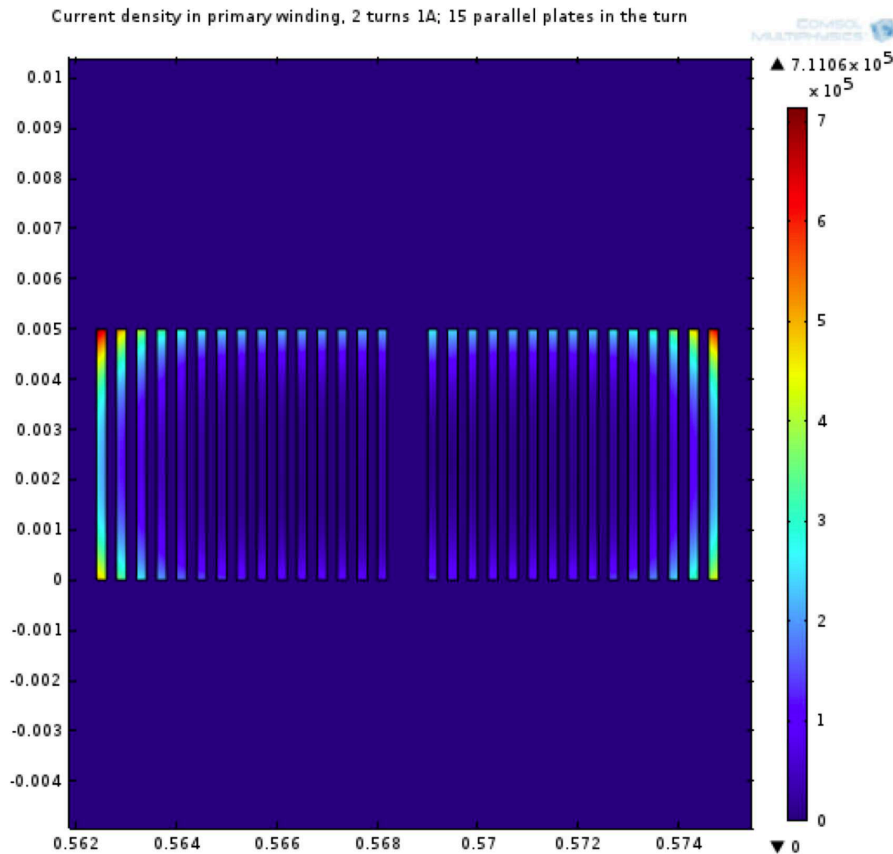


Figure 2.24: The current density in the primary winding when it is fed with 1A.

The innermost and the outermost plates in the primary winding will have high current density, about  $6 \cdot 10^5 \text{ A/m}^2$  shown as red spots in the figure. Most of the plates will have 1 to 2 times the dc current density resulting in a total resistance of 3 times the dc resistance at 20 kHz.

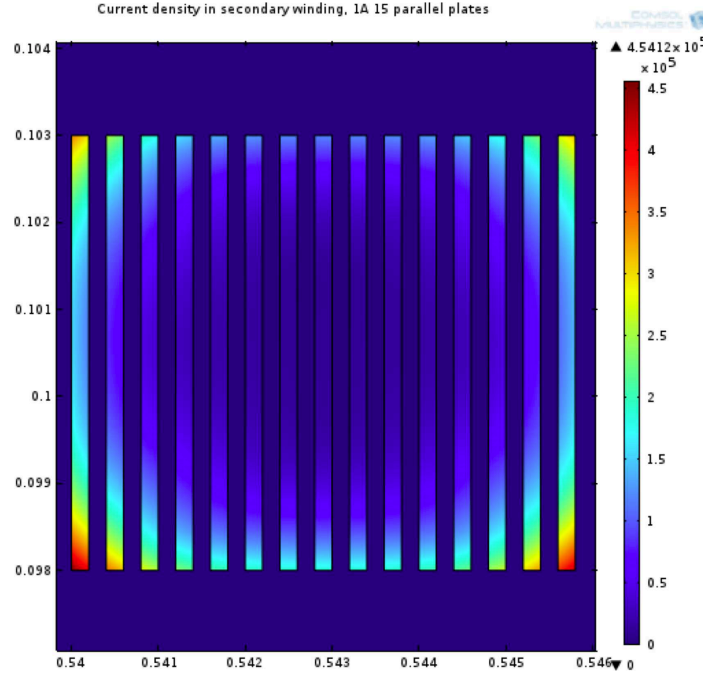


Figure 2.25: The current density in the secondary winding when it is fed with 1A.

The innermost and the outermost plates in the secondary winding will have high current density, about  $4 \cdot 10^5 \text{ A/m}^2$  shown as red spots in the figure. Most of the plates will have almost the dc current density, resulting in a total resistance of 2.3 times the dc resistance at 20 kHz.

It is possible to lessen the high resistance (skin effect) by decreasing the B-field around the wires. The boundary condition for high frequencies,  $\mathbf{J}_s = \hat{n} \times \mathbf{H}_{\text{outside}}$ , where  $\mathbf{J}_s$  = the surface current density,  $\mathbf{H}_{\text{outside}}$  = the H-field outside the conductor and  $\hat{n}$  the normal to the surface. Moving the outer conductors away from the other will lessen the B around the outer conductors and thus the skin effect. See [1] and [2].

### 2.2.2 Parameters

From the simulations we get the following values of inductances and resistances.

**Primary** winding:  $N_1=2$  turns.  $L_1=31.17 \mu\text{H}$ ,  $M=9.44 \mu\text{H}$ ,  $R_1=37.4 \text{ m}\Omega$

**Secondary** winding:  $N_2=1$  turn.  $L_2=7.84 \mu\text{H}$ ,  $R_2=13.3 \text{ m}\Omega$  and  $v_{\text{ind}_2}=1.186 \text{ V}$  for  $i_1=1 \text{ A}$  and  $f=20 \text{ kHz}$ . The new coupling factor will be  $k_{\text{new}}=0.60$

The maximum possible induced voltage in winding 2,  $v_{\text{ind}_2, \text{max}} = \omega M_{\text{max}} i_1 = 1.218 \text{ V}$ , is higher than the simulated, because the secondary winding was not placed exactly at the radius where  $M=M_{\text{max}}=9.69 \mu\text{H}$ .

These parameters from simulations are used in the next section about resonant coupling. For a better positioning of the secondary winding  $k_{\text{new}, \text{max}}=0.62$ .

### 2.2.3 Comparison of models

By using the coupling factor  $k_{\text{new}}$  on the circular and helix coils in Chapter 3 Table 3.3.3 we find the values of  $k_{\text{new}}$  for the two simulations in 3D 0.65 (circular coils), 0.60 (helical coils) and for 2D 0.70 (circular coils).

For one of the transformers used in Chapter 4 we find in Table 4.1  $M=42 \mu\text{H}$  and  $L_2=58 \mu\text{H}$  giving  $k_{\text{new}}=0.72$  approximately.

## 2.3 Resonant coupling

Let us use resonant capacitors in our magnetically coupled circuits, see Figure 2.26! We are using capital letters for the complex quantities voltages  $V$  and currents  $I$ .

At **resonance** the energy will oscillate between the inductance and the capacitance. The electric field will remain between the plates of the capacitor, but the magnetic field will be outside the loop. The field is a **near field** close to the loop. If we put another loop with the same resonant frequency close to the first one, energy will be transmitted to this circuit.

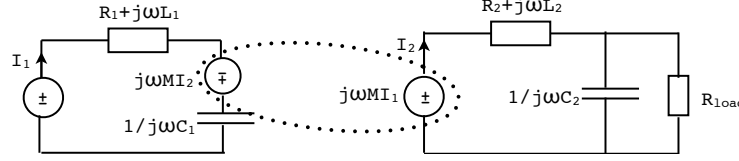


Figure 2.26: Equivalent circuit for the two coupled loops including two resonant capacitors and a resistive load  $R_{load}$  in circuit 2, symbolizing a current loop on the ground and a pick-up circuit on board a vehicle.

In our case  $R_2 = 0.0133 \ll \omega L_2 = 0.985 \Omega$ . We can neglect  $R_2$  and redraw the right part of the circuit, see Figure 2.27!

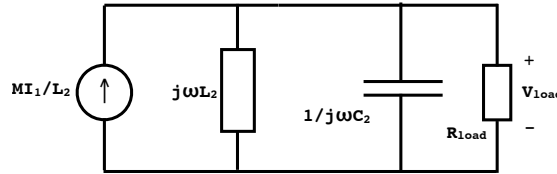


Figure 2.27: The right part of the circuit, the pick-up circuit, redrawn

### Power to the load

Let us calculate the maximum power transferred to a load using the same circuits without and with the capacitors  $C$ .

The voltage  $V_{load} = (M/L_2)I_1 Z = (M/L_2)I_1 / Y$ , where  $Z = 1/Y$  = the impedance seen by the current source. The admittance  $Y = 1/j\omega L_2 + j\omega C_2 + 1/R_{load}$

At resonance we have  $1/\omega L_2 = \omega C_2$  and  $V_{load} = (M/L_2)I_1 R_{load}$

The power to the load will then be

$$P_{load} = R_{load} [(M/L_2)|I_1|]^2 = R_{load} [(N_1/N_2)k_{new}]^2 |I_1|^2 \quad (2.5)$$

**Numerics:**  $R_1 = 37.41 \text{ m}\Omega$ ;  $L_1 = 31.17 \text{ }\mu\text{H}$ ;  $M = 9.44 \text{ }\mu\text{H}$ ;  $R_2 = 13.31 \text{ m}\Omega$ ;  $L_2 = 7.84 \text{ }\mu\text{H}$ ;  $I_1 = 25 \text{ A}$  (rms);  $f = 20 \text{ kHz}$ ;  $C_2 = 8.1 \text{ }\mu\text{F}$ ;  $R_{load} = 1.5, 10, 15, 20 \Omega$ , see Table 2.2!

Table 2.2: Power to the load without and with a tuning capacitor for different loads

$R_{load} \Omega$	$Q_2$	$P_{without C} \text{ kW}$	$P_{resonant C} \text{ kW}$
1.5	1.54	0.410	1.36
10	10.2	0.087	9.04
15	15.2	0.058	13.6
20	20.3	0.044	18.1

At parallel resonance the transferred power will be about  $1 + Q_2^2 \approx 3$  to 400 times bigger than without  $C_2$ !  $Q_2 = R_{load} / \omega L_2$

A high  $Q$  will need a high  $R_{load}$  or a low  $L_2$ . But we need a high  $M$  for a high current in the pick-up circuit! More turns in primary loop will give a higher  $M$ , if  $N_2 = 1$ . The calculations above are done for  $N_1 = 2$  and  $N_2 = 1$ .

### Currents in the windings

The load current  $I_{load} = (N_1/N_2)k_{new}I_1$  will also be the current through the secondary winding at resonance. A high  $N_1$  will give a high  $I_2$ .

### Frequency dependence

At resonance the load power is independent of the frequency. However the frequency must be high enough to fulfill the requirements in the calculations above:

1.  $R_2 \ll \omega L_2$  ;
2. We must be able to find a capacitor for the resonant condition  $C_2 = 1/(\omega^2 L_2)$

The higher the frequency, the more influence from the skin effect in the windings.

## 2.4 Conclusions of Chapter 2

Higher currents will need a better winding design. One way to lessen the skin effect in the winding layers is to move the innermost and outermost layer away from the rest of the layers. See for instance Figure 2.25. This will lessen the B-field around the wires and thus the highest induced currents in these layers.

A horizontal displacement of 5 cm at a height of 10 cm will diminish the load power with approximately 7 % .

Ferrite plates will improve  $k_{\text{new}}$  and thus the maximum possible current in the secondary loop. Big ferrite plates will give 3 times the power to a load compared to loops in air.

Changing the vertical distance between the two loops from 5 cm to 10 cm will lessen the maximum possible power to a load with 42% for air. Using big ferrite plates the same change in distance will lessen the maximum possible power to a load with 25%.

The coupling factor  $k_{\text{new}}$  will give a way to compare the efficiency of the different geometries and materials in the coil design.

Adding a resonant C to the secondary circuit the maximum transferred power will go up 3 to 400 times.



## Chapter 3

# Modelling the wireless transfer coil system into Ansys

A general wireless transfer coil system is modelled in the finite element program package Ansys Maxwell, similar to that shown in Figure 3. The set-up consists of two coils, one transmitting coil and one receiving coil. Adjacent to both coils there is a ferrite plate and an aluminium plate. The model in Figure 3 is two-dimensional with axial symmetry, so that the coils are represented as a set of circular coils, rather than a helix coil. A helix coil is also a possibility. Therefore, three-dimensional models are used to represent the problem set-up.

The 3D models are made with both helix coils and a set of circular coils in order to compare 2D and 3D models. The models are verified against analytical calculations [2] and also to some extent against a master thesis work [3] where a similar set-up is used. The purpose of the models is to calculate inductance values and resistances when skin effect and proximity effects are considered. The results are also compared to measured results from a bachelor work [4], where a part of the problem set-up (the emitting coils) is shown in Figure 3.2.

The solution types "transient" and "eddy current" were both used for 2D as well as 3D problems. The transient solution considers the time difference of the magnetic fields, induced voltages etc., allowing any kind of time-dependence, and consequently allowing several transmitting coils with different frequencies. On the other hand, the eddy current solver allows only magnetic fields varying sinusoidally in time (with one frequency); thus solving the steady-state problem. The displacement currents are in all cases neglected.

The model set-up, solution and post-processing are made with a script, written in Visual Basic within Microsoft Excel. Therefore, the input variables and dimensions can be varied from an Excel sheet.

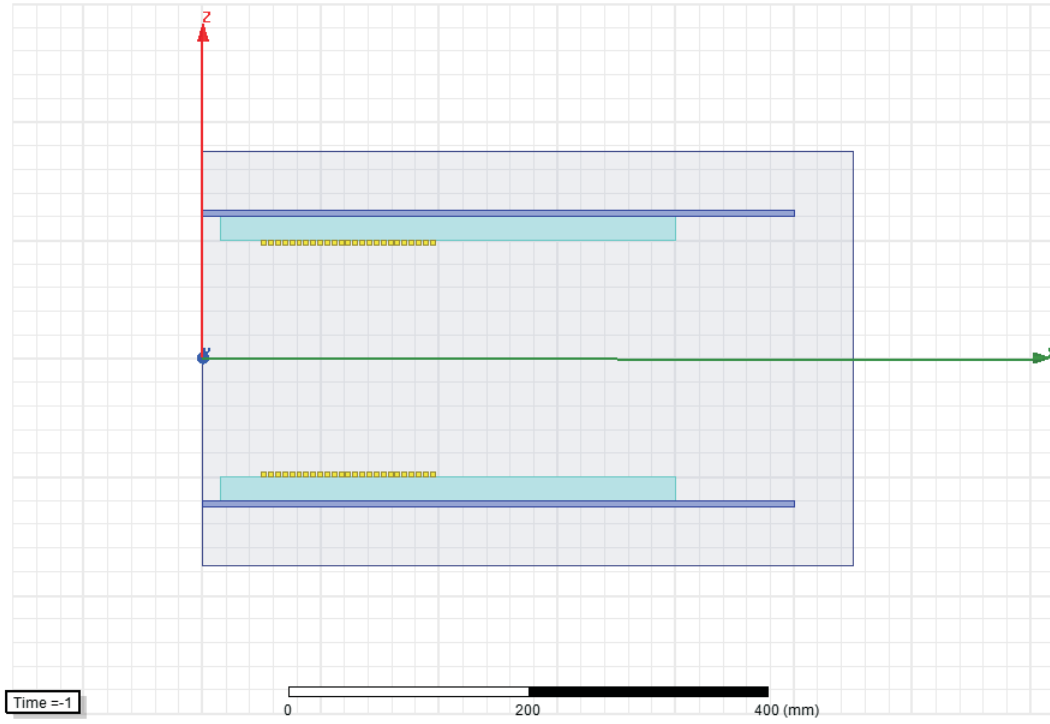


Figure 3.1: The general problem set-up in Maxwell with one emitting and one receiving coil (yellow), each on a ferrite plate (light blue) which in turn is placed on a plate of aluminium (purple).

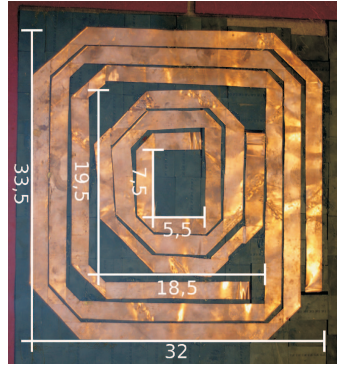


Figure 3.2: The emitting coils used in [4]

### 3.1 Verification against analytical problems

Simple problems were modelled in 2D, 3D, with transient as well as with eddy current solutions, in order to compare the results for the different solutions and in order to compare with analytic calculations when applicable. In this way, the model solutions can be verified. The resistance is calculated from the power loss,  $P_{\text{loss}}$  and the input current,  $I$ , as

$$R = \frac{P_{\text{loss}}}{I^2} \quad (3.1)$$

where the power loss is Solid Loss in Maxwell, and it can only be calculated if eddy effects are set for the material where the loss is to be calculated. For the transient solutions, it should be noted that the power loss is varying in time, so that the mean value of the power loss should be used in (3.1). It is also important to model several periods, so that steady state is achieved and considered. Likewise, it is important to have a sufficient number of time-steps per period.



If the conductors are stranded, then Stranded Loss instead of Solid Loss is to be used to find  $R$  in (3.1). In [3], the resistance is calculated as the real part of the induced emf over the input current. This is a somewhat risky method as the emf is found from derivation of the flux linkage which can easily introduce errors. Also, the phase shift between the emf and the current may be very close to  $90^\circ$  (when the power factor is close to zero), introducing even more risk of errors.

Further, the resistance can also be found from the impedance calculations done in Maxwell when using the eddy current solution. Then, the inductance is also found. It is also possible to let Maxwell calculate the inductance matrix for the transient solutions. Otherwise, the inductance is best calculated as induced flux linkage over input current,

$$L = \lambda/i \quad (3.2)$$

It is important to have a good mesh: It is especially important to have a good mesh for problems with a high frequency where the skin effect in a conductor is to be modelled. Maxwell allows a mesh operator that considers the skin effect. This mesh operator is appropriate to use on the surface of the conductor. Maxwell will calculate the skin depth at a given frequency and you can set the number of layers and the maximum size of the finite elements.

The boundary conditions are handled with an air box surrounding the problem region, yielding a default boundary condition that means that no magnetic flux leaves the boundary. In those cases where a part of the problem region is modelled, then symmetry boundary conditions are used.

### 3.1.1 One long coil

One very long coil with a circular cross section is modelled in 2D, as seen in Figure 3.1.1. The result of the inductance and resistance per length is compared to a similar example [2]. The coil has a radius of  $a = 2$  mm; it is fed with an ac current of 1A rms and it is surrounded with air. Transient and eddy current solutions are used for the frequencies 50 Hz and 100 kHz. The result at 100 kHz may be calculated analytically [2] as

$$R = \frac{\ell}{\sigma \pi a^2} \left[ \frac{1}{4} + \frac{a}{2\delta} \right] \quad (3.3)$$

Equation (3.3) is valid when the skin depth is smaller or equal to half the coil radius. The skin depth,  $\delta = 0.209$  mm at 100 kHz and the conductivity,  $\sigma = 5.8 \cdot 10^7$  and a relative permeability equal to 1. The result from the different solver options are shown in Table 3.1 for the frequency of 100 kHz.

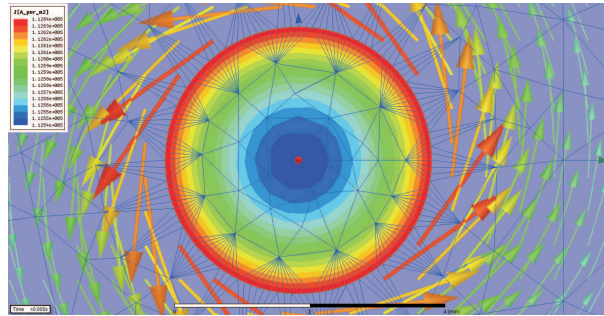


Figure 3.3: One very long current-carrying coil with a circular cross section with the magnetic field shown with arrows around the coil and the current density distribution due to skin effect shown with the colour plot. It is also possible to see some of the mesh lines indicating a denser mesh at the surface of the coil.

As can be seen in Table 3.1, the analytical calculation of  $R$  is similar to the solutions given by Maxwell, within a maximum discrepancy of 2.5 %. Further the value of the inductance (not calculated analytically) vary not more than 8% between solution methods.

Table 3.1: Resistance and inductance values at 100 kHz of a long coil

	Analytically	Maxwell eddy current solver		Maxwell transient solver	
Resistance/length [m $\Omega$ /m]	6.91	$R(P_{\text{loss}}) = 6.92$	$R(Z)=6.92$	$R(P_{\text{loss}}) = 6.74$	$R(Z) = \text{NA}$
Inductance/length [nH/m]	-	$L(\lambda)=250$	$L(Z)=261$	$L(\lambda) = 265$	$L(\text{matrix}) = 300$

### 3.1.2 One ring coil

One ring coil with a rectangular cross section is modelled in 3D as well as with an axisymmetric 2D model. The coil carries a current of 1A at a frequency of 5 kHz. The model is seen in Figure 3.1.2. The analytical solution, using (3.3) is an approximation as the expression used is for a straight coil with a circular cross section with radius 5 mm and with a mean length ( $l$ ) of one turn equal to  $2\pi \cdot 25$  mm. Dimensions are: Inner radius 20 mm, outer radius 30 mm, and height 10 mm. The results are seen in Tables 3.2 and 3.3 showing reasonable coherence (< 16%, difference), except for the matrix calculation from the 2D transient solver. The skin depth,  $\delta$  is 0.93 mm at 5 kHz and the conductivity,  $\sigma$  is  $5.8 \cdot 10^7$  and the relative permeability is equal to 1.

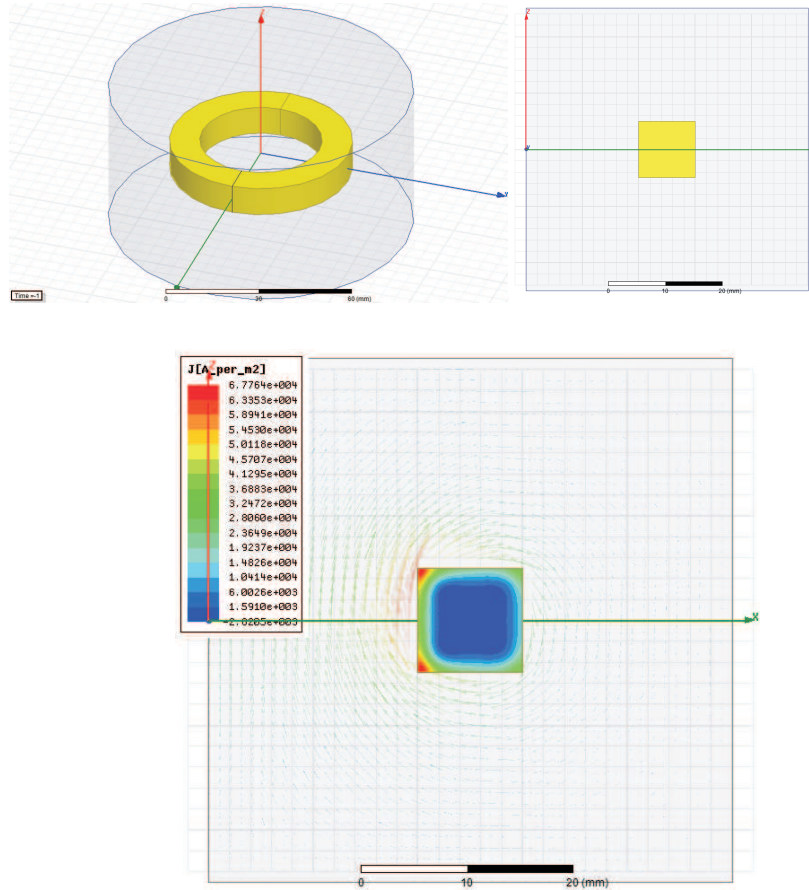


Figure 3.4: One ring coil with a rectangular cross section surrounded with an air box. The 3D model is to the upper left and the 2D axisymmetric model is to the upper right whereas the resulting current density is shown for the 2D model in the lower part of the figure.

Table 3.2: Resistance and inductance values at 5 kHz of a ring coil. From a 3D model

	Analytically	Maxwell eddy current solver		Maxwell transient solver	
Resistance [ $\mu\Omega$ ]	101	$R(P_{\text{loss}}) = 106$	$R(Z) = 92$	$R(P_{\text{loss}}) = 84.5$	$R(Z) = \text{NA}$
Inductance [nH]	—	$L(\lambda) = 39$	$L(Z) = 43$	$L(\lambda) = 47.5$	$L(\text{matrix}) = 45.25$

Table 3.3: Resistance and inductance values at 5 kHz of a ring coil. From a 2D model

	Analytically	Maxwell eddy current solver		Maxwell transient solver	
Resistance [ $\mu\Omega$ ]	101	$R(P_{\text{loss}}) = 96$	$R(Z) = 96$	$R(P_{\text{loss}}) = 94$	$R(Z) = \text{NA}$
Inductance [nH]	—	$L(\lambda) = 39$	$L(Z) = 42$	$L(\lambda) = 44$	$L(\text{matrix}) = 1850$

### 3.1.3 Two ring coils

Two ring coils with a rectangular cross section is modelled as solid coils, calculating the resistance, the self inductance and the mutual inductance and the coupling coefficient. The lower coil carries a current of 1A at a frequency of 5 kHz whereas the upper coil carries no current. The model is seen in Figure 3.1.3, and the results are seen in Tables 3.4 and 3.5.

The resistances seem to increase due to proximity effects compared to the case with one coil only. Looking at the tables it may be observed that the results coincide fairly well with one clear exception: The results from the transient 2D model gives totally strange values from the inductance matrix calculations. The same solution gives reasonable values of the inductance when calculated from the flux linkage. Considering this, it is advisable to calculate the parameters in several different ways. It may be observed that the 2D transient solution gives more reasonable values of the inductances if the coils are set to be stranded instead of solid coils ( $L_{\text{self}} = 50$  nH and  $L_{\text{mutual}} = 23$  nH, compared to stranded coils and 3D transient solutions;  $L_{\text{self}} = 51$  nH and  $L_{\text{mutual}} = 22$  nH ).

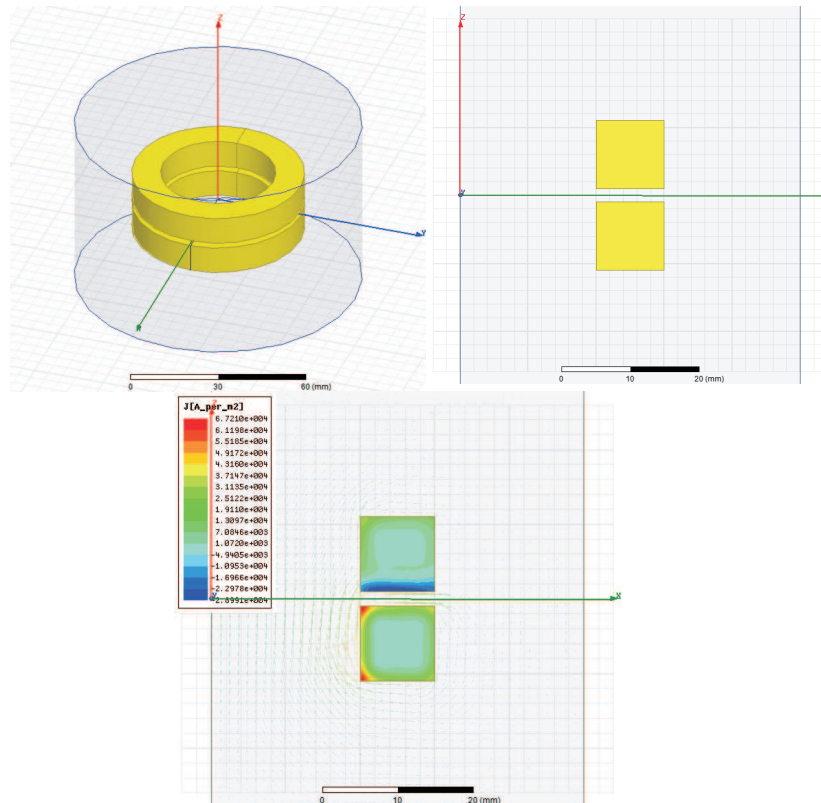


Figure 3.5: Two ring coils with a rectangular cross section surrounded with an air box. The 3D model is to the upper left and the 2D axisymmetric model is to the upper right whereas the resulting current density is shown for the 2D model in the lower part of the figure.

Table 3.4: Resistance and inductance values at 5 kHz of two ring coils. From a 3D model.

	Maxwell eddy current solver 3D		Maxwell transient solver 3D	
Resistance [ $\mu\Omega$ ]	$R(P_{\text{loss}}) = 107$	$R(Z) = 123$	$R(P_{\text{loss}}) = 110$	$R(Z) = \text{NA}$
Self inductance [nH]	$L(\lambda) = 37.4$	$L(Z) = 39.5$	$L(\lambda) = 43.4$	$L(\text{matrix}) = 40.0$
Mutual inductance [nH]	$L(\lambda) = 20.8$	$L(Z) = 21.8$	$L(\lambda) = 22.7$	$L(\text{matrix}) = 23.0$
Coupling coefficient	0.549		0.542	

Table 3.5: Resistance and inductance values at 5 kHz of two ring coils. From a 2D model.

	Maxwell eddy current solver 2D		Maxwell transient solver 2D	
Resistance [ $\mu\Omega$ ]	$R(P_{\text{loss}}) = 94.3$	$R(Z) = 127$	$R(P_{\text{loss}}) = 124$	$R(Z) = \text{NA}$
Self inductance [nH]	$L(\lambda) = 36.5$	$L(Z) = 38.5$	$L(\lambda) = 40.0$	$L(\text{matrix}) = 1850$
Mutual inductance [nH]	$L(\lambda) = 21.6$	$L(Z) = 22.1$	$L(\lambda) = 22.1$	$L(\text{matrix}) = 842$
Coupling coefficient	0.574		0.55	

### 3.2 Comparison to a master thesis work; two ring coils with Ferrite and aluminium plates

One of the examples in [3] is used in order to compare results. The set-up, see Figure 3, consists of two copper coils with 25 turns ( $\mu_r = 1$  and  $\sigma = 5.8 \cdot 10^7$ ), one transmitting coil and one receiving coil. Symmetry may be used to constrain the problem region to half, having the symmetry line along the x-axis. This is used for the resistance calculations. However, then you cannot calculate mutual inductance. Each coil cross section has a radius of 3.94 mm, according to [3]. However, the coils are represented with square cross section areas in the Maxwell models, as seen in Figure 3. Adjacent to both coils there is a ferrite plate ( $\mu_r = 1000$  and  $\sigma = 1$ ) and an aluminium plate ( $\mu_r = 1$  and  $\sigma = 3.54 \cdot 10^7$ ). The material properties are constant and the problem is thus linear. The frequency is 40 kHz. The dimensions are given in [3]. The skin depth of the copper coils,  $\delta_{\text{Cu}} = 0.33$  mm at 40 kHz, and the skin depth of the aluminium and ferrite plates are,  $\delta_{\text{Al}} = 0.42$  mm and  $\delta_{\text{Fe}} = 79.5$  mm, also at 40 kHz.

The coils in [3] are made of 200 strands of Litz-wire with a strand diameter of 0.2 mm, so that the Litz-wire does not eliminate the skin effect but reduce it. This poses some problems when calculating the resistance, as the Litz-wire cannot practically be modelled as twisted, solid strands. Therefore, the coils are either modelled as 25 stranded coils with 1 turn (assuming that the Litz-wire cancels out the skin effect completely) or as 25 solid coils with 1 turn (assuming that there is full skin effect despite the Litz-wire). The true value of the resistance should then be between those found values.

There is also a question on what cross section area to choose for the coil. The coil radius is 3.94 mm giving an area of  $\pi(3.94)^2 \text{ mm}^2$ . However, with the Litz-wire considered, the area can be as small as  $200 \cdot \pi(0.2)^2 \text{ mm}^2$  with a fill factor of 100%. Using a square cross section area, both cases are considered with two different values of the side of the square; 3.94 mm and 2.5 mm. The coils are in both cases treated as solid coils, yielding a resistance of  $1.2 \Omega$ , and  $0.6 \Omega$  respectively. The latter value is for the smaller cross section area. It would seem strange that the smaller cross section area gives a lower resistance. However, the smaller area gives a larger distance between coils and thus a smaller impact of the proximity effect.

If the same problems are solved with stranded coils, then the smaller cross section area gives a higher resistance (yielding a resistance of  $0.022 \Omega$ , and  $0.054 \Omega$  respectively where the latter value is for the smaller cross section area). It could therefore be concluded that if the coils have no skin and proximity effects, then the resistance may be as low as  $0.022 \Omega$ , whereas if the coils are solid coils, and the proximity and skin effect is not minimized at all, then the resistance may be as high as  $1.2 \Omega$ . The resistance is in all cases calculated from the power loss (either solid loss or stranded loss), as in eq. (3.1). However, in [3], the resistance is calculated (to be  $0.1 \Omega$ ) as the real part of the induced voltage over the input current.

To calculate the inductance, the coils are modelled as stranded coils, thereby minimizing the calculation time for the 3D transient solution and allowing a 2D transient solution. This is considered to be a reasonable approach as the inductance values are not much affected by the skin and proximity effects, as was seen in Section 3.1.2, although the self inductance was 20% higher for the stranded coils compared to the solid coil. The coils have a square cross section area with length 3.94 mm. When modelling the problem as a steady state problem (with the eddy current solver), the 25 coils cannot be coupled to a winding, and thus is the inductance for the whole winding complicated to calculate, using the 25 inductance-values. Therefore, the inductance is calculated from energy,  $W$ ,

$$W = \frac{1}{2} Li^2 \quad (3.4)$$

yielding a value of  $280 \mu\text{H}$  for the self inductance. This may be compared to a 3D transient solution with solid coils yielding a self inductance of  $277 \mu\text{H}$ , a mutual inductance of  $56 \mu\text{H}$ , and a resistance of  $0.12 \Omega$ . The plot of the flux density from a 2D eddy current solution is shown together with a plot of the flux density from the transient 2D solution, showing very similar results, see Figure 3.2. Figure 3.7 shows the flux density distribution for the case with a 3D transient solution with solid coils. The impedance values are further calculated only from the transient solutions (both in 3D and 2D) with stranded coils, and the results are listed in Table 3.6 together with the results of [3]. In both Table 3.6 and Figures 3.2 and 3.7 and for values mentioned above, the results are similar regarding flux pattern and the inductances, whereas the resistance values are more astray due to the difficulty to model the Litz-wire properly.

Table 3.6: Resistance and inductance values at 40 kHz of two stranded ring coils with 25 turns.

	Maxwell transient solver 3D		Maxwell transient solver 2D		[3]
Resistance [ $\Omega$ ]	$R(P_{\text{loss}}) = 0.023$		$R(P_{\text{loss}}) = 0.02$		0.1
Self inductance [ $\mu\text{H}$ ]	$L(\lambda)=282$	$L(\text{matrix})=282$	$L(\lambda)=278$	$L(\text{matrix}) = 273$	280
Mutual inductance [ $\mu\text{H}$ ]	$L(\lambda)=57$	$L(\text{matrix})=57$	$L(\lambda)=57$	$L(\text{matrix}) = 58$	55



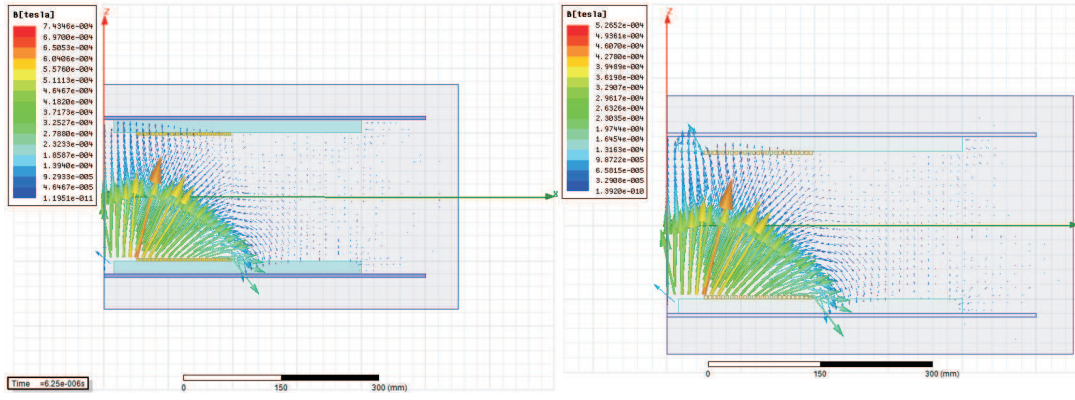


Figure 3.6: The flux density distribution from the transient 2D solution (left) and from the eddy current 2D solution (right).

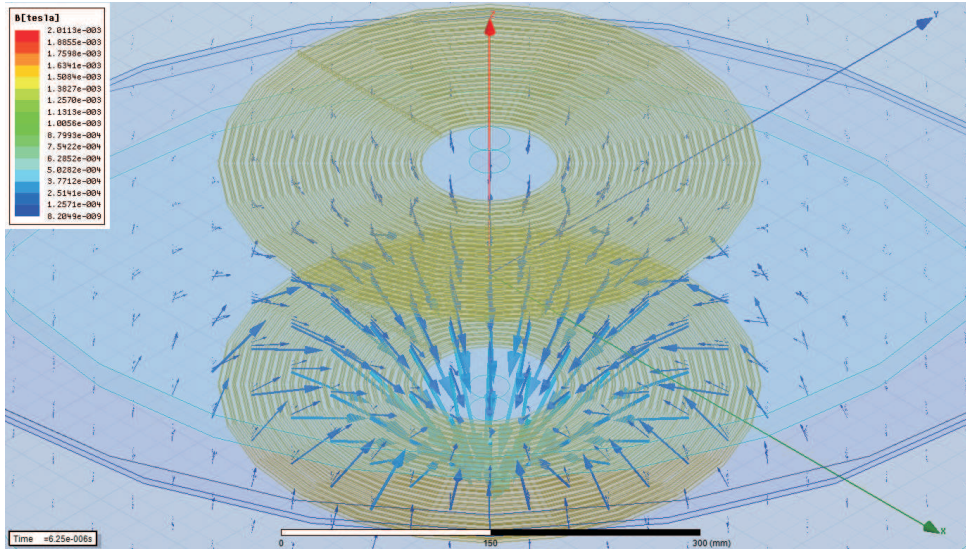


Figure 3.7: The flux density distribution for the 3D transient solution with solid coils.

### 3.3 Comparison to a bachelor thesis work; a flat helix coil with 3 turns

A wireless charging system for a go-cart was built and analysed in [4]. The same system was modelled here in order to compare results and in order to develop the electromagnetic modelling of wireless charging systems. Similar dimensions and values of material properties and frequencies as in [4] are thus used. However, to start with, the coils which are helix coils with rectangular shapes, as shown in Figure 3.2, are modelled as circular solid coils with a 2D transient model, as shown in Figure 3.3, where the resulting flux density distribution with currents in the (lower) emitting coils is shown.

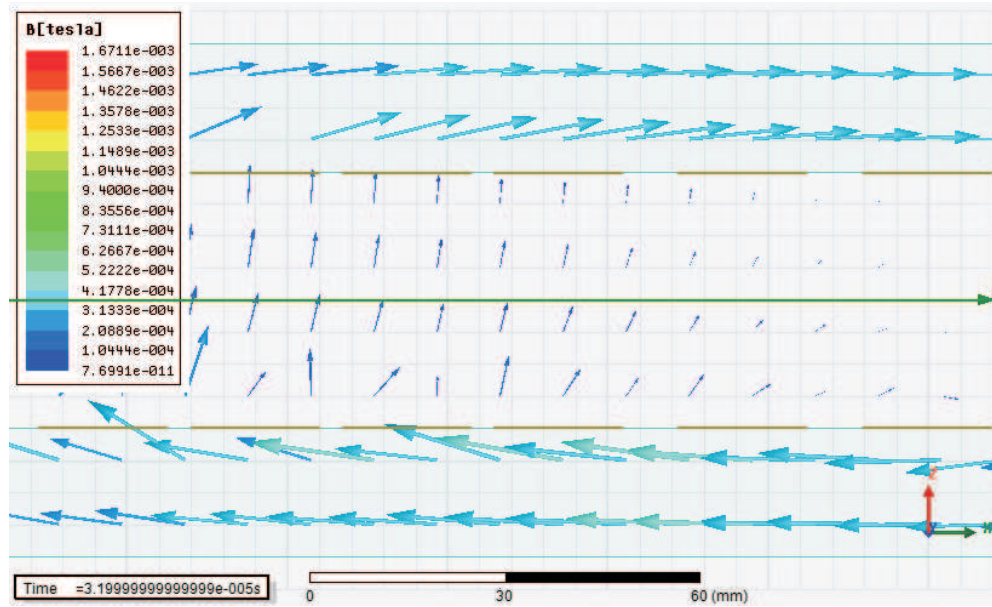


Figure 3.8: The wireless charger with two lower emitting windings with three turns each and a similar receiving coil set, with attached ferrite plates. The arrows show the flux density distribution due to currents in the emitting windings, with a frequency of 100 kHz for the inner winding and 40 kHz for the outer winding.

### 3.3.1 2D axisymmetric transient model of a flat circular coil with 3 turns

The wireless charging system consists of two emitting coils and two receiving coils, all four coils having 3 turns. The coils are attached to a ferrite plate with a relative permeability of 1600. The coils are made of copper sheets with dimensions 0.2·20 mm. The dimensions of the emitting coils in [4] are seen in Figure 3.2. The dimension used for the circular coils are chosen so that the area of the emitting coils are similar. The receiving coils are modelled as mirrors of the emitting coils. See the used dimensions in Table 3.7.

Table 3.7: Dimensions of the wireless charging emitting coils used for the 2D model.

INNER COIL:	
Inner radius of inner emitting coil	36.2 mm
Distance between turns	3.7 mm
Outer radius of inner emitting coil	103.5 mm
OUTER COIL:	
Inner radius of outer emitting coil	107.2 mm
Distance between turns	8.75 mm
Outer radius of outer emitting coil	184.7 mm
FERRITE PLATE:	
Ferrite plate outer radius	350 mm
Ferrite plate height	20 mm
Distance between upper and lower coils	40mm

The results of the inductance and resistance values are shown and compared to the measured values in [4], in Table 3.8. The dc resistance of the coils are measured to be around 10-20 mΩ , according to [4]. The calculated value from the model with circular coils at 50 Hz is 5.6 mΩ for the inner emitting coil and 11.8 mΩ, for the outer emitting coil. It is said in [4] that the coils are not much affected by the skin and proximity effects due to the thinness of the copper conductors.

However, according to the simulations, the ac resistance at 100 kHz (37 mΩ) is about 7 times larger than the resistance at 50 Hz (5.6 mΩ). The effect may also be seen in Figure 3.9 and Figure 3.10 showing the current density distribution of the inner emitting coil at 100 kHz and outer emitting coil at 40 kHz, respectively.

From Table 3.8 it may be seen that the simulated values of the inductances are not very close to the measured values in [4]. This is believed to be due to the simplification of the model, assuming the coils to be separate turns with circular shapes, instead of the helical coils with rectangular shapes as in [4]. Also, the gap between coils in [4] is uncertain and here only assumed to be 40 mm.

Table 3.8: Resistance and inductance values for the emitting coils from the 2D transient model compared to [4]

	2D transient model	[4]
INNER COIL AT 100 kHz:		
Resistance [ $m\Omega$ ]	37	-
Self Inductance [ $\mu H$ ]	3.3	3.4
Mutual Inductance [ $\mu H$ ]	2.3	1.4
OUTER COIL AT 40 kHz:		
Resistance [ $m\Omega$ ]	128	-
Self Inductance [ $\mu H$ ]	11	8
Mutual Inductance [ $\mu H$ ]	8.8	6.5

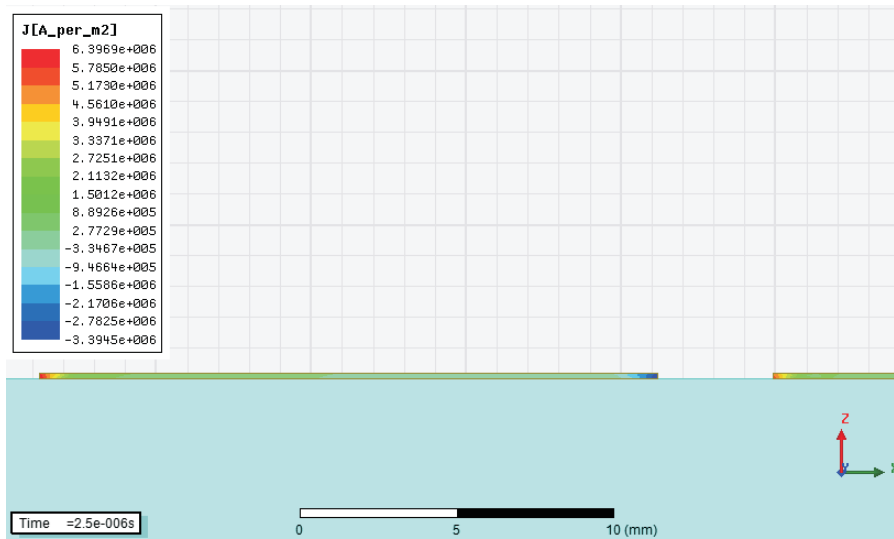


Figure 3.9: The current density distribution of the inner emitting coil at 100 kHz.

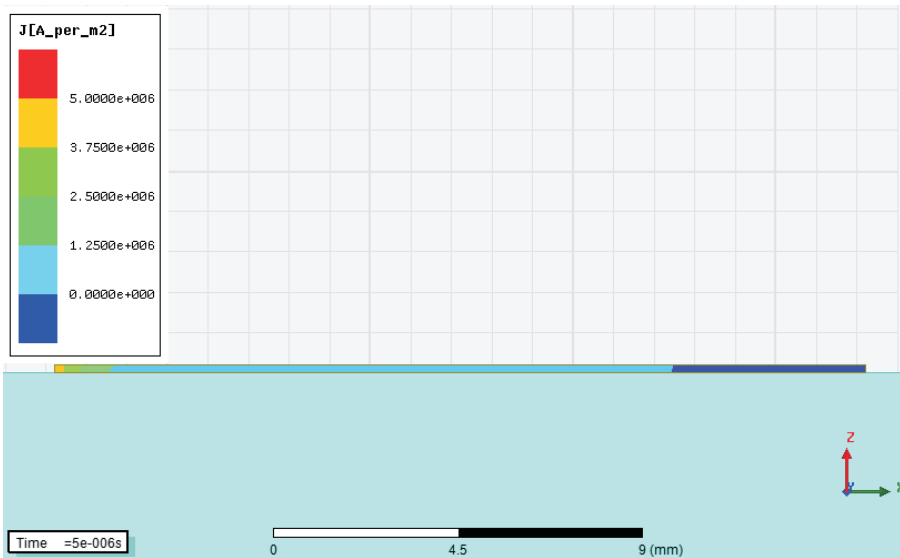


Figure 3.10: The current density distribution of the outer emitting coil at 40 kHz.



### 3.3.2 A 3D transient model of a flat circular coil with 3 separate turns

In order to compare a helical coil model with a model with separate turns, a 3D model is made consisting of the inner windings of the model shown in Figure 3.3, see Figure 3.3.2. The resulting values of resistance, self-and mutual inductances are found in Table 3.3.2. The skin effect may be seen in Figure 3.12 showing the induced currents in the windings. The mesh used was rather coarse with no mesh refinement operators. As can be seen in Table 3.3.2, the resistance value from the 3D model is much smaller than from the 2D model whereas the inductance values coincide more. The discrepancies are believed to be due to the coarse mesh.

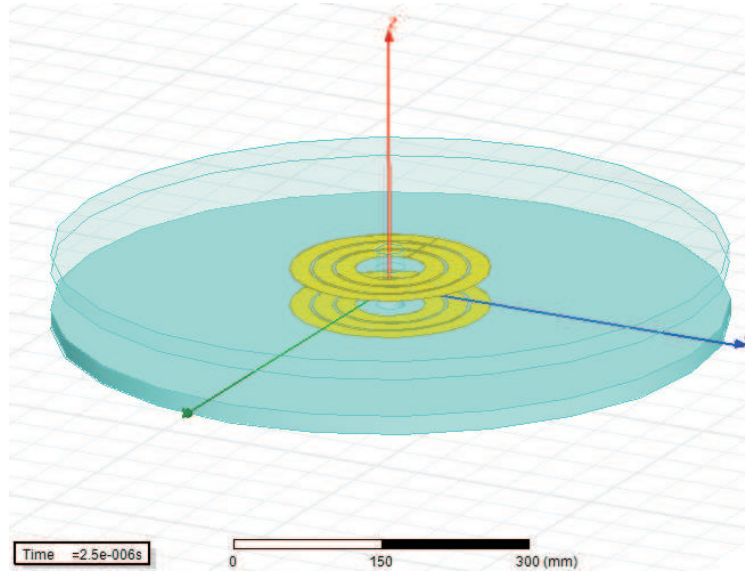


Figure 3.11: The 3D model of the inner windings and ferrite plates (the upper ferrite plate is made transparent).

Table 3.9: Resistance and inductance values for the inner emitting coils from the 3D transient model compared to the 2D transient model

	3D	2D
INNER COIL AT 100 kHz:		
Resistance [ $\text{m}\Omega$ ]	15	37
Self Inductance [ $\mu\text{H}$ ]	3.4	3.3
Mutual Inductance [ $\mu\text{H}$ ]	2.2	2.3

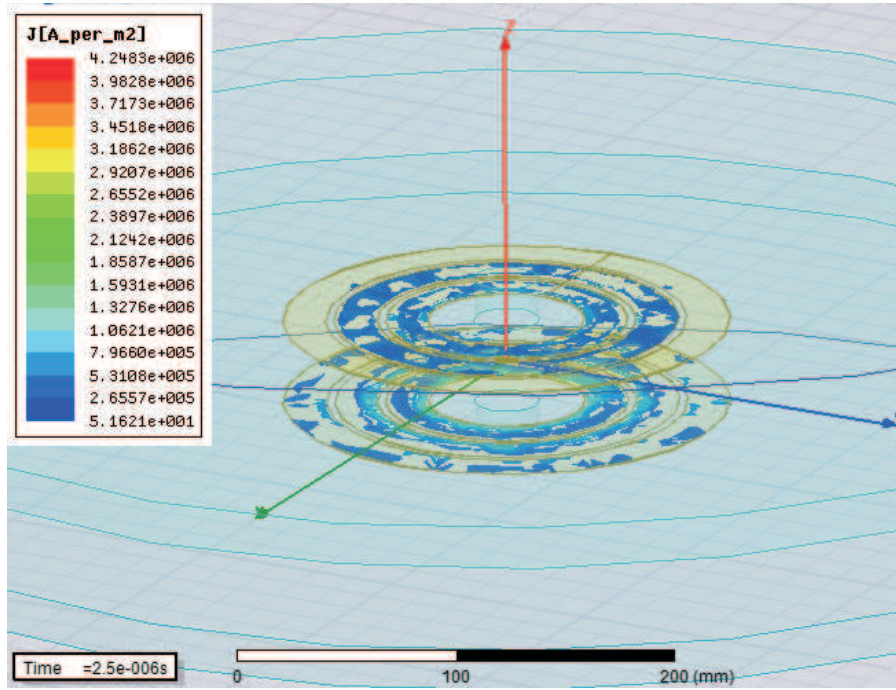


Figure 3.12: Current distribution in the coils at 100 kHz.

To minimize the problem further, only the emitting inner coil is modelled using a symmetry boundary condition, see Figure 3.3.2. The symmetry boundary condition forces the field on the boundary to be normal to the boundary. This is quite reasonable as may be seen in the 2D model in Figure 3.3, where it can be seen that the flux density is mostly normal to the symmetry line. Then, it must be considered that the calculation of the resistance from the solid loss gives the resistance for both windings (emitting and receiving) so that the resistance of the emitting winding is half the calculated value. The same goes for the inductance calculated from the induced flux; half the calculated value is the self inductance of the emitting winding. Thus, (3.1) and (3.2) is modified to

$$R = \frac{P_{\text{loss}}}{2I^2} \quad (3.5)$$

$$L = \frac{\lambda}{2i} \quad (3.6)$$

when using symmetry. The resulting values of resistance, self-and mutual inductances are found in Table 3.3.2. The mesh used was again rather coarse with no mesh refinement operators. As can be seen in Table 3.3.2, the values of the resistance and self inductance are somewhat similar to the other results (from the 3D model without symmetry and from the 2D model). The discrepancies are once again believed to be due to the coarse mesh.

Table 3.10: Resistance and inductance values for the inner emitting coils from the 3D transient models (with and without symmetry) compared to the 2D transient model

	3D without symmetry	3D with symmetry	2D
INNER COIL AT 100 kHz:			
Resistance [mΩ]	15	13	37
Self Inductance [μH]	3.4	2.8	3.3
Mutual Inductance [μH]	2.2	-	2.3

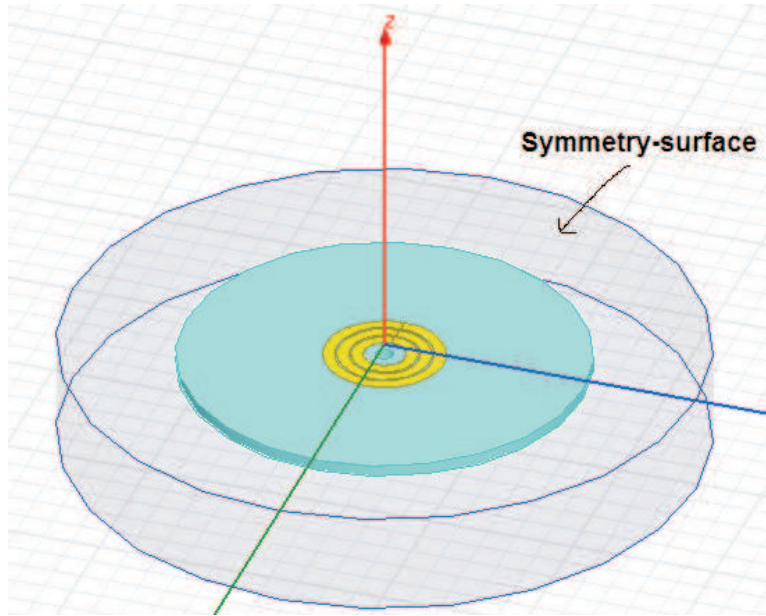


Figure 3.13: The 3D model with a symmetry boundary condition, modelling the lower inner winding and ferrite plate.

### 3.3.3 A 3D transient model of a flat helix coil with 3 circular turns

Two helical coils with three circular turns each are drawn in a 3D model, consisting of the inner winding of the model shown in Figure 8. The helical coils are shown in Figure 3.3.3. To see the similarities between the helical coil and the coils with three separate turns (as is modelled in 3.3.2), all coils are drawn in the same picture, see Figure 3.15. The difficulty with a model of a helical coil is to extend the coil to the outer boundaries of the model, so that the terminal surfaces are coinciding with the outer boundary. Therefore, the helical coil ends are extended through the ferrite plate until the outer boundary of the air box. The ferrite plates have openings where the coil ends are led through the plates.

The resulting values of resistance, self-and mutual inductances are found in Table 3.3.3. The mesh used was again rather coarse with no mesh refinement operators. The resistance should be somewhat higher than for the circular coils due to the additional length of the coils needed to create terminals at the air box boundary. This is also the fact, as seen in Table 3.3.3, when comparing the two 3D solutions. The inductance values are also somewhat higher for the helix coils compared to the separate circular coils.

It should be noted that by leading the coil ends through the ferrite, there is induced flux in the ferrite plate in the tangential direction, circulating around the z-axis (in the x-y-plane). This flux density component was not induced for the circular coils. The induced flux density is shown in Figure 3.16, and the induced current density is shown in Figure 3.17.

Table 3.11: Resistance and inductance values for the inner emitting helical coil from the 3D transient models compared to the 3D and 2D transient models with three circular coils

	3D circular coils	3D helical coils	2D
INNER COIL AT 100 kHz:			
Resistance [ $m\Omega$ ]	15	17	37
Self Inductance [ $\mu H$ ]	3.4	4.0	3.3
Mutual Inductance [ $\mu H$ ]	2.2	2.4	2.3

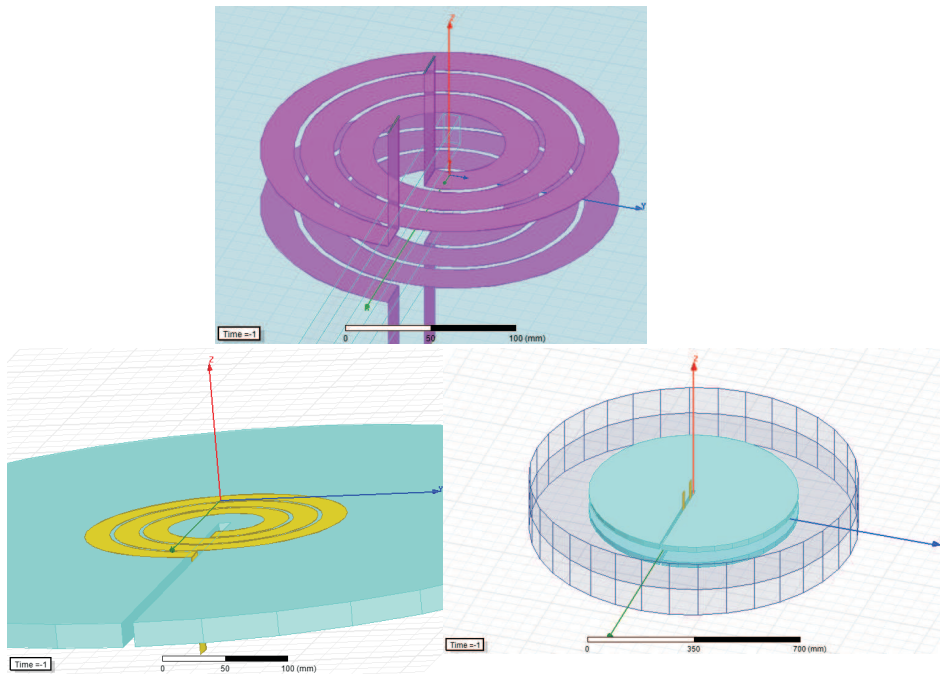


Figure 3.14: Two helix coils attached to ferrite plates, and surrounded with an air box. The ferrite plates (light blue) have openings where the coil ends are extended to the outer boundary of the air box.

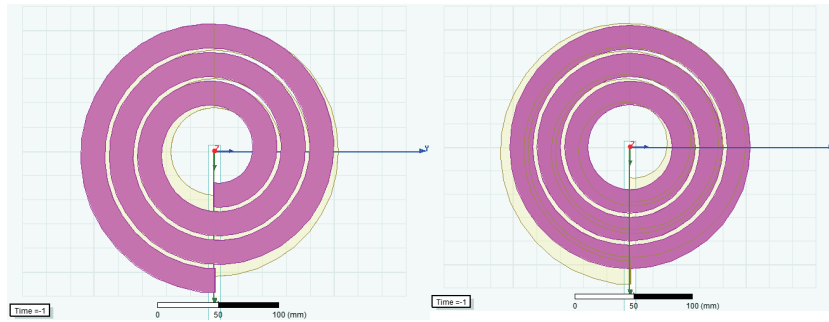


Figure 3.15: The helix coil compared to the three separate coils used in section 3.3.2

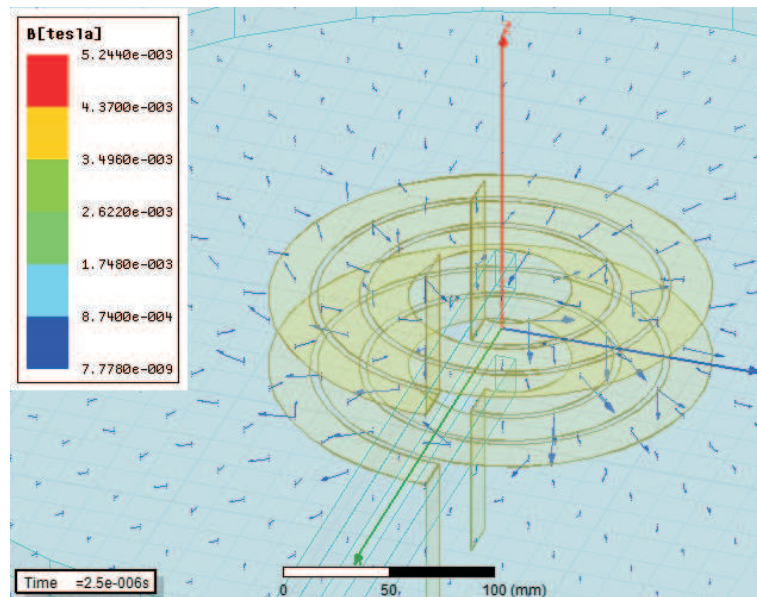


Figure 3.16: Flux density distribution in the helix coils at 100 kHz



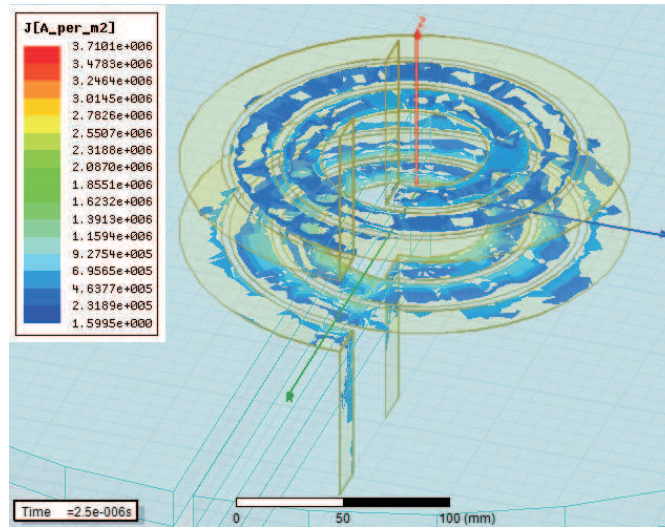


Figure 3.17: Current distribution in the helix coils at 100 kHz.

### 3.3.4 A 3D transient model of a flat helix coil with 3 rectangular turns

A rectangular helical coil with three turns is made in a 3D model, consisting of the inner emitting winding of the model shown in Figure 3.3. The rectangular helical coil is shown in Figure 3.3.4. To see the similarities between the rectangular helical coil and the circular helical coil (as is modelled in 3.3.3), both coils are drawn in the same picture, see Figure 3.3.4. Just like for the circular helix coil, the rectangular helix coil have coil ends extended through the ferrite plate until the outer boundary of the air box, supposedly yielding a somewhat higher resistance due to the extended coil length.

The resulting values of resistance, self- and mutual inductances are found in Table 3.3.4. The mesh used was again rather coarse with no mesh refinement operators. As seen in Table 3.3.4, when comparing the two 3D solutions, the resistances as well as the inductance values are somewhat higher for the rectangular helix coils compared to the circular helix coils. This is due to the increased length of the rectangular coil compared to the circular coil. The induced flux density is shown in Figure 3.20, and the induced current density is shown in Figure 3.21. When using 50 Hz instead of 100 kHz, the inductance values are about the same whereas the resistance value becomes as low as 8.3 mΩ more than half the value than that at 100 kHz as seen in Table 3.3.4.

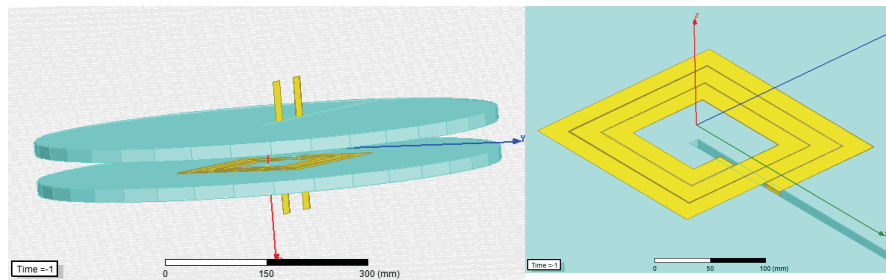


Figure 3.18: Two helix coils attached to ferrite plates, and surrounded with an air box. The ferrite plates (light blue) have openings where the coil ends are extended to the outer boundary of the air box.

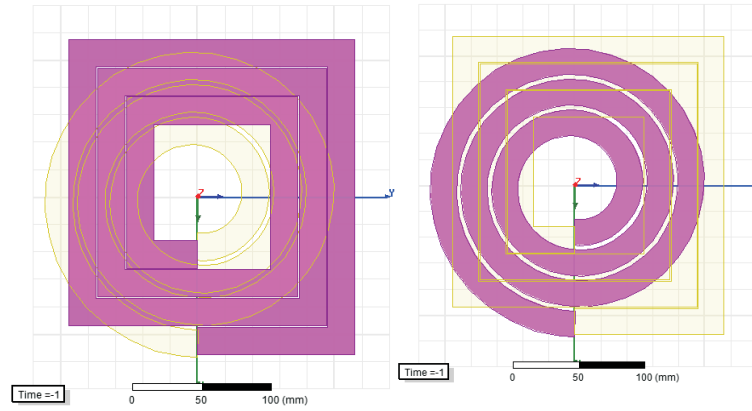


Figure 3.19: The rectangular helical coil compared to a circular helical coil used in section 3.3.3

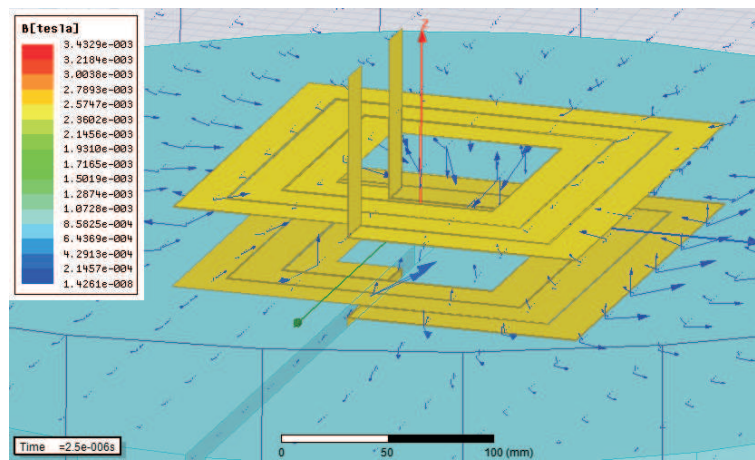


Figure 3.20: Flux density distribution in the rectangular helix coils at 100 kHz.

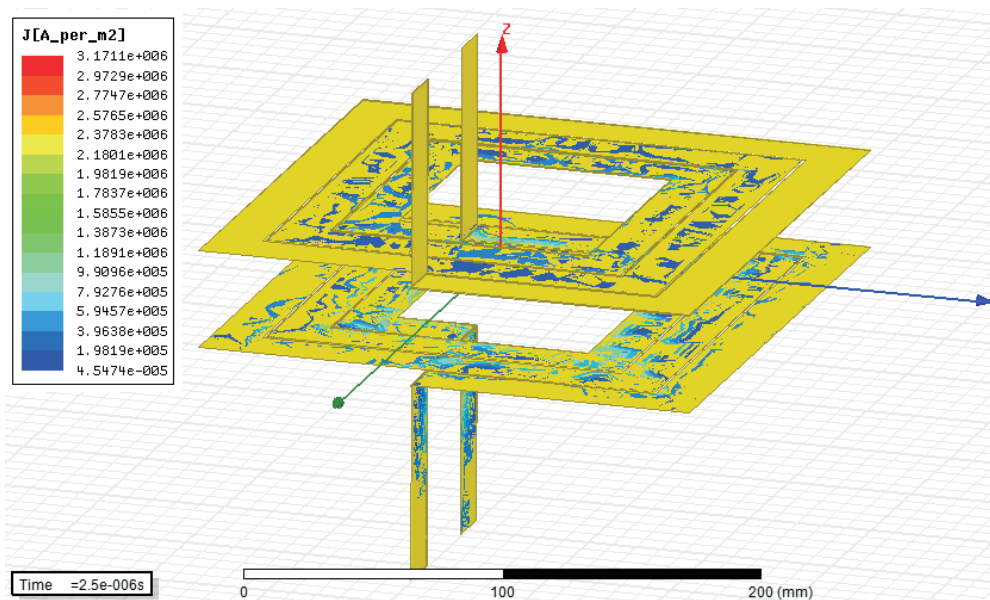


Figure 3.21: Current distribution in the rectangular helix coils at 100 kHz..

Table 3.12: Resistance and inductance values for the inner emitting rectangular helical coil from the 3D transient models compared to the 3D transient model with circular helical coil and the 2D transient model

	3D rectangular helical coil	3D circular helical coil	2D
INNER COIL AT 100 kHz:			
Resistance [ $m\Omega$ ]	24	17	37
Self Inductance [ $\mu H$ ]	5.6	4.0	3.3
Mutual Inductance [ $\mu H$ ]	3.7	2.4	2.3

### 3.3.5 A 3D eddy current model of a flat helix coil with 3 rectangular turns with finer mesh

As it was not feasible to solve with a refined mesh for the 3D transient problem described in the last section, the same problem is solved with an eddy current solver. This allows a much faster solution (minutes instead of hours) and a possibility to use mesh operators to refine the mesh. The resulting values of resistance, self-and mutual inductances are found in Table 3.3.5.

The mesh operators used were skin depth operator on the coils and length based on the air box. Both the initial mesh and the refined mesh are shown in Figure 3.22. In Table 3.3.5 it is seen that the mesh refinement does not make a big difference when the frequency is 50 Hz whereas for the high frequency of 100 kHz, the value of the resistance is changing a lot depending on the mesh quality.

Table 3.13: Resistance and inductance values for the inner emitting rectangular helical coil from the 3D eddy current model compared to the 3D transient model

	3D transient	3D eddy current coarse mesh	3D eddy current fine mesh
INNER COIL AT 100 kHz:			
Resistance [ $m\Omega$ ]	24	29	58
Self Inductance [ $\mu H$ ]	5.6	5.2	5.0
Mutual Inductance [ $\mu H$ ]	3.7	3.5	3.3
INNER COIL AT 50 Hz:			
Resistance [ $m\Omega$ ]	8.3	8.2	8.1
Self Inductance [ $\mu H$ ]	6.1	6.1	6.0
Mutual Inductance [ $\mu H$ ]	4.1	4.2	4.1

### 3.3.6 Comparison to a bachelor thesis work; two frequencies

Two emitting coils with different frequencies are modelled in the 2D axisymmetric transient model described in 3.3.1. Currents of 1 A is set for the emitting coils, with 100 kHz for the inner coil and 40 kHz for the outer coil. The input currents are seen in Figure 3.3.6. The resulting flux linkages in the receiving coils are shown in Figure 3.3.6, and the induced voltages in Figure 3.3.6.

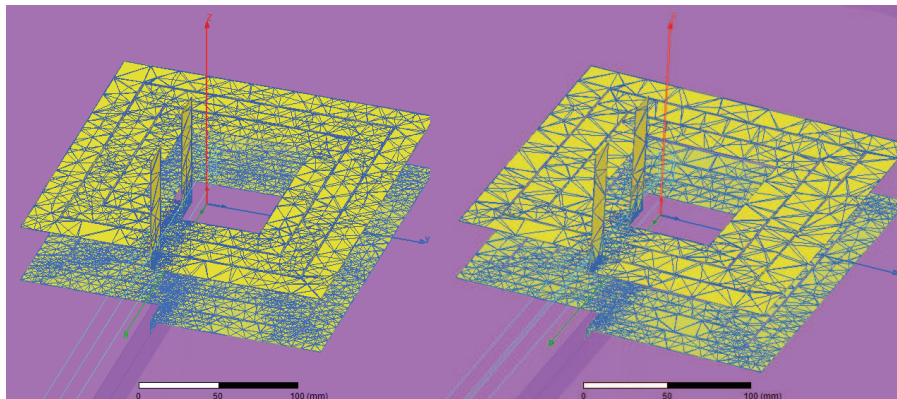


Figure 3.22: Refined (left) and initial (right) mesh used for the eddy current solver.

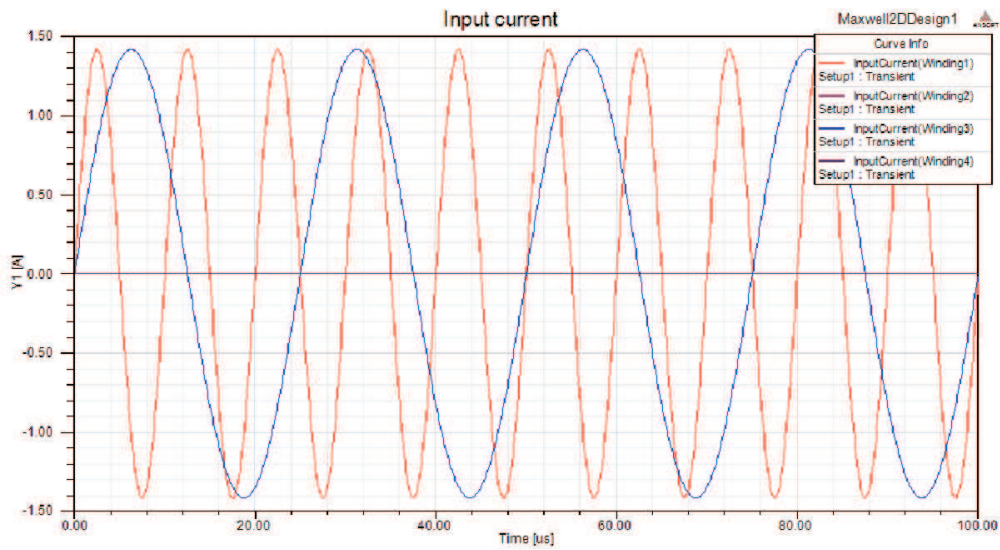


Figure 3.23: Input current. Winding 1 is the inner emitting winding with 100 kHz ac current of 1 A. Winding 3 is the outer emitting winding with 40 kHz ac current of 1 A. Winding 2 and 4 are the receiving windings.

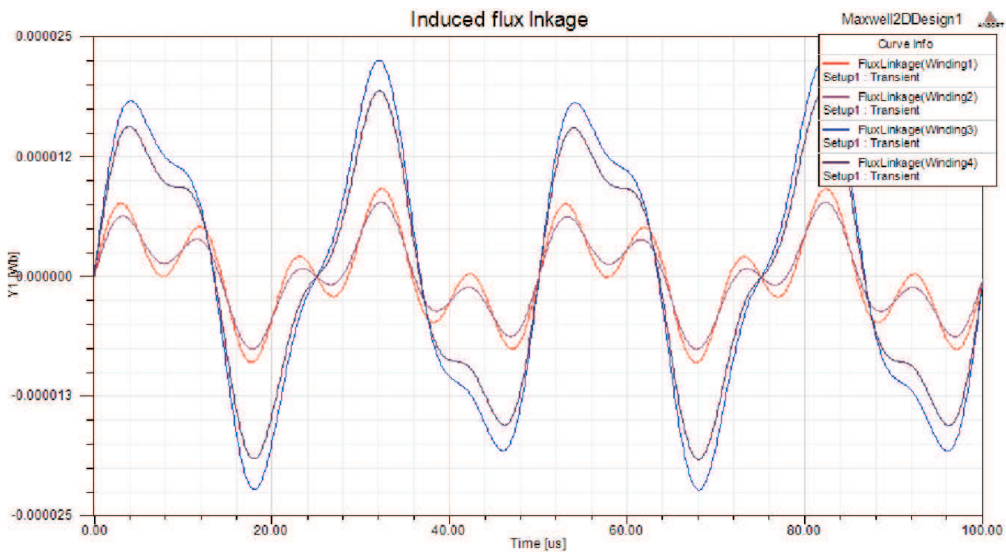


Figure 3.24: Induced flux linkage. Winding 1 is the inner emitting winding with 100 kHz ac current of 1 A. Winding 3 is the outer emitting winding with 40 kHz ac current of 1 A. Winding 2 and 4 are the receiving windings.



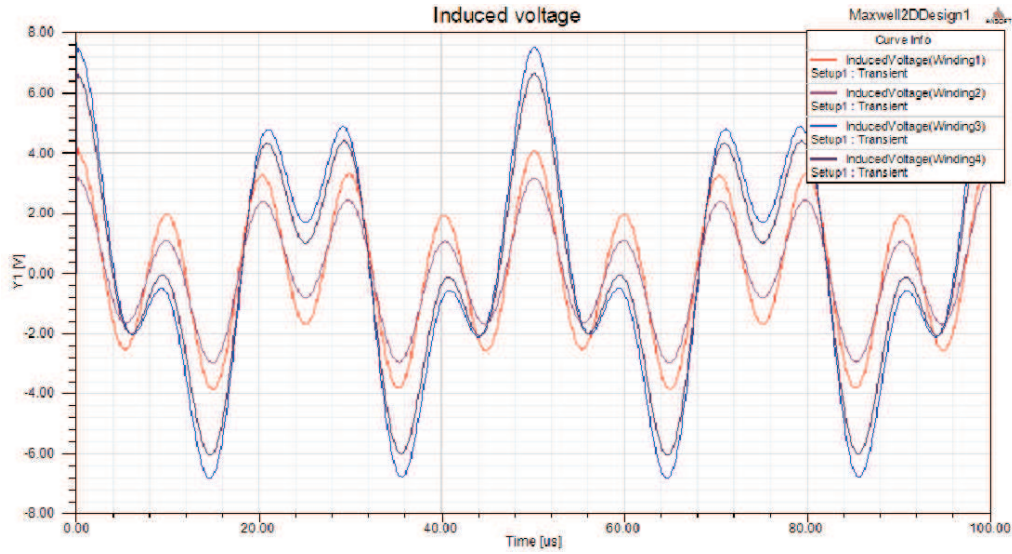


Figure 3.25: Induced voltage. Winding 1 is the inner emitting winding with 100 kHz ac current of 1 A. Winding 3 is the outer emitting winding with 40 kHz ac current of 1 A. Winding 2 and 4 are the receiving windings.

### 3.4 Conclusions of Chapter 3

Differently shaped coils may be modelled, and resistance and inductance values calculated, even with several coils with different frequency of the input currents (if using a transient solver). However, it must be remembered the importance of the mesh quality, especially for the calculation of the resistance at high frequencies. This was shown clearly in Table 3.3.5, where the high frequency resistance values varied by 60 % between a dense mesh and a course mesh, whereas the low frequency resistance and inductance were more similar (11% difference) for both mesh densities. Also, it is important to compare results with different solvers, measurements, and if possible with analytical calculations.

In this work the calculation of resistance with FEM programs was compared with analytical calculations (for two simple examples), showing a small discrepancy, (less than 3 % when cases were identical and less than 16 % when the FEM model were similar to the conditions for the analytical calculations). When comparing with measurements the discrepancy was larger, which could be explained with the complicated helix coils, necessitating a simplified 3D model. Still both the resistance and inductance values were shown to be rather similar for FEM calculations and measurements. When comparing the results for a 25-coil system [4] the difference was small (< 5%) regarding inductance, whereas the resistance values were more astray due to the difficulty to model the Litz-wire properly.



## Chapter 4

# Wireless charger unit

### 4.1 Overview of charger

In inductive chargers, the incoming grid voltage is first rectified to a DC-link voltage. After this, the voltage is chopped to a high-frequency voltage that feeds the primary coil or a resonant circuit. The resonant circuits are used to minimize switching losses in the transistors and compensate for reactive power in inductive components. The most straightforward method is to use an ordinary H-bridge, [5]. See Figure 4.1. How to connect capacitors have been studied in [5] and Wang et.al. recommends a parallel resonant circuit both on the primary and the secondary side of the transformer.

A different approach is used where a series coupled capacitor compensate the reactive effect of the primary coil. The series capacitor blocks possible DC-offset that otherwise should produce a high magnetizing current. On the secondary side a parallel capacitor compensate the leakage inductance.

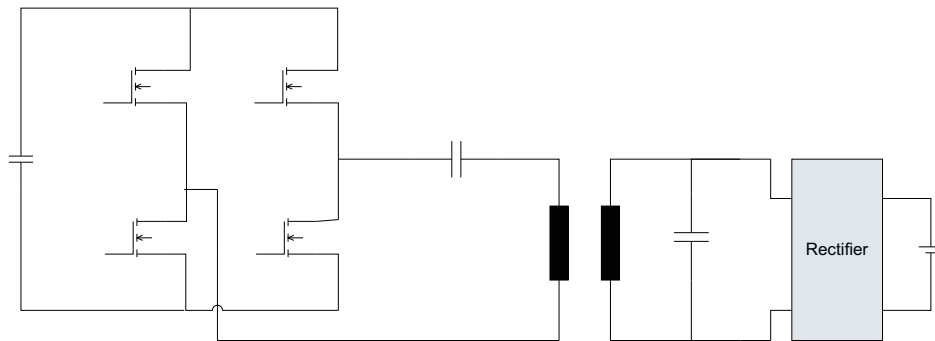


Figure 4.1: H-bridge, implemented in Simulink

Another way is to use just one leg of the H-bridge and connect the other branch of the primary circuit to a mid-point of the dc-link capacitor. See Figure 4.2

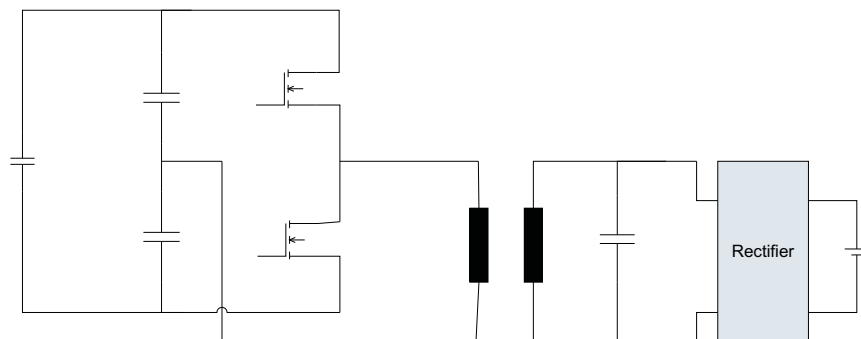


Figure 4.2: Simplified primary circuit.

In this section we will study a case with a 100 kW power level, which is a suitable level for charging a plug-in bus.

Incoming voltage is 400 V  $\pm$  10 % which means that the DC-link voltage has a nominal value of  $U_{dc} = 540 - 650V$ , depending on if we have a diode rectifier or a transistor converter. We assume a battery voltage that is changing between 250 V and 400 V depending on state of charge.

## 4.2 Transformer

There are some different ways to construct the transformer.

1. Concentric coils
2. 'Transformer' with large air gap
3. Flat winding in the air gap

When designing the transformer it is important to have low leakage and that the flux passes from the primary to the secondary in a 'smart' way. If it passes through the conductors there will be unnecessary losses in the winding.

The concentric coil, see Figure 4.3 works rather well, the winding is concentrated and the flux will pass inside of the winding, but the leakage flux is high. The solution has been used by HBT Datensysteme with an efficiency of 90 % but with rather low power density, 2-3 kW/m<sup>2</sup>. The low power density is reflected by the low inductance per unit length,  $l = 1.3 \mu H/m$ , for each turn of the winding. The transformer types are compared with an air gap of 3 cm between the primary and secondary side.

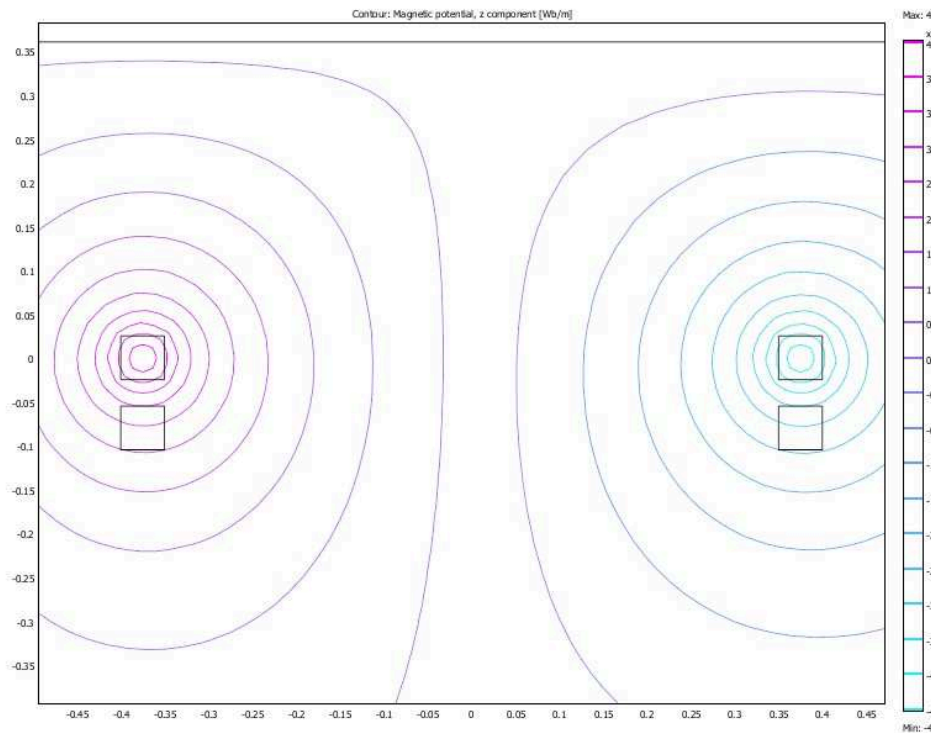


Figure 4.3: Concentric coils.

The second one is to make an 'ordinary' transformer with a large air gap, See Figure 4.4.

Although the air gap is large the inductance increases to  $l = 6.4 \mu H/m$

In this type there is a specific volume for the winding and the flux is guided through soft magnetic parts, both in the centre and in the outside of the construction. In this way the flux is lead around the conductor area and eddy currents in the winding may be lowered. On the other hand more core parts are exposed to the varying flux and the iron core losses will be higher.

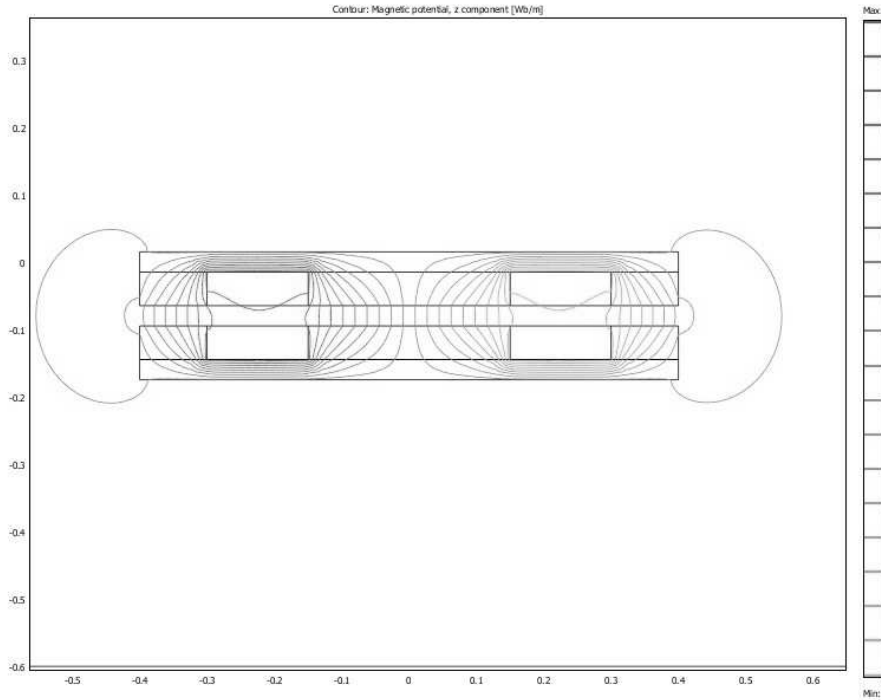


Figure 4.4: 'Transformer Type'.

The third type is a completely flat structure with the winding placed in between the two core parts, see Figure 4.5!

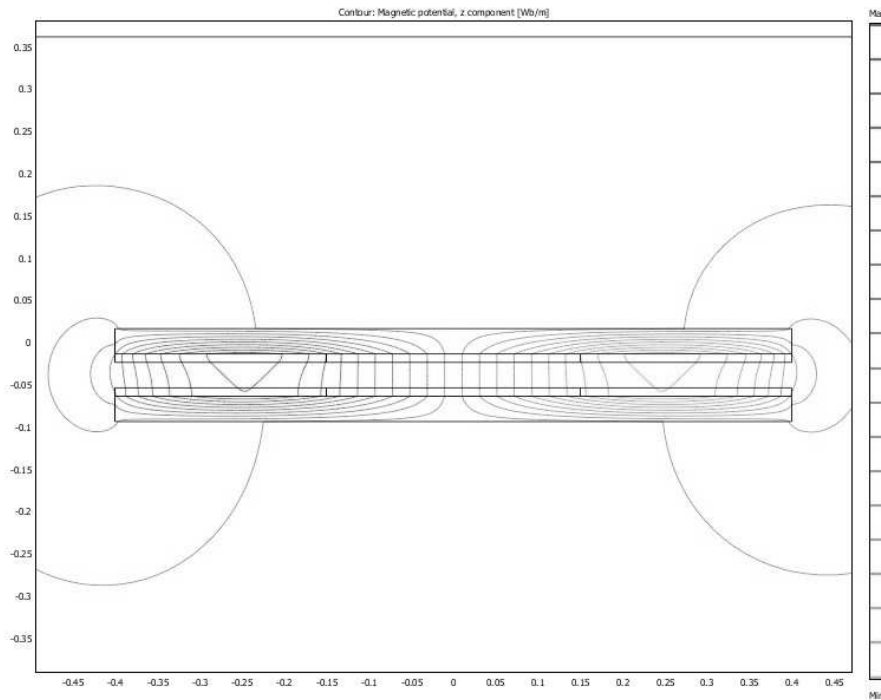


Figure 4.5: Flat winding. Helix type.

This transformer will be very flat but has the disadvantage of high flux through the winding. If the winding is made of large conductors or strips the eddy current losses will be high. The inductance value is anyway rather high,  $l = 3.8 \mu\text{H/m}$ .

The transformer type has more space for the winding and the useful flux is 4-5 times the flux of a helix coil. In order to find a suitable size of the transformer as well as the number of turns, an approximate calculation of the transformer is done.

Consider the cross section of a rectangular transformer according to Figure 4.6.

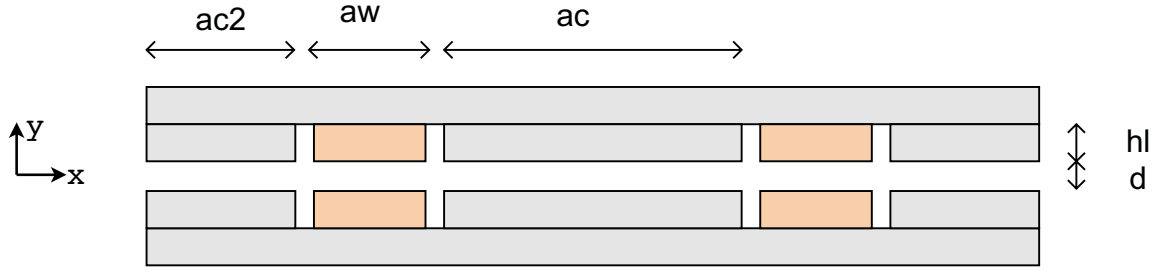


Figure 4.6: Cross section of a rectangular transformer.

A: Outer width of transformer

$a_c$ : Width of centre

$a_w$ : Width of winding area

$d$ : Length of air gap

$h_l$ : Thickness of winding

$\ell_c$ : The length of the centre core in z-direction

Assume that the winding is divided in  $N$  number of turns. As a start it is assumed that the number of turns is equal in the primary and secondary winding. We analyse the magnetic field and all variables denotes the peak (instantaneous) value. It may also denote the rms-value, but in that case the magnetizing current must also be a rms-value.

The area of each conductor will be:

$$A_{Cu} = h_l \frac{a_w}{N}$$

In the primary conductor flows the current  $I$ . Ampere's law will give, if we assume infinite permeability of the iron core,

$$2dH_d = NI$$

The flux density is,

$$B_d = \mu_0 H_d \quad (4.1)$$

and the linked magnetic flux is

$$\Psi = NB_d \ell_c a_c$$

The induced voltage, is

$$E = \omega \Psi = \omega \mu_0 \frac{N^2 I a_c \ell_c}{2d}$$

We calculate the mutual inductance as the linked flux divided by the current,

$$L_m = \frac{\Psi}{I} = \mu_0 \frac{N^2 a_c \ell_c}{2d} \quad (4.2)$$

The leakage inductance is found from two-dimensional FEM-analysis and it is weakly depending on the winding thickness. The leakage flux varies some percent when varying the winding thickness and a rough figure is 28 % in this transformer type.

A common system voltage is  $U_n = 400$  V (rms) and in that case we need at least  $I_n = 250$  A (rms) in order to produce the nominal power of  $P_n = 100$  kW.

The voltage across the leakage inductance is

$$U_\lambda = \omega L_\lambda I$$

The voltage across the leakage inductance limits the power and also sets the necessary insulation class of the system. The optimal value is hard to find, but a rough estimate is that this voltage component should be limited to 400 V (rms).

$$L_\lambda < 400/(\omega I)$$

For a current  $I=250$  A(rms) and a frequency  $f=25$  kHz,  $L_\lambda$  should be lower than  $10 \mu\text{H}$ . In the equivalent circuit  $L_\lambda$  is divided into two parts,  $L_{\lambda,1}$  and  $L'_{\lambda,2}$ . With the assumption that the leakage is 28% of the main flux, we find that  $L_m$  should be around  $36 \mu\text{H}$ .

### Calculations on the transformer in Figure 4.6. Results are presented in Table 4.1

**1. The inductances:** The geometric quantities for the transformer are given in the table. Assuming  $N=7$  (equal number of turns in the primary and secondary windings), equation (4.2) will give  $L_m = 42 \mu\text{H}$ . For 28% leakage flux the two equal leakage inductances  $L_{\lambda,1} = L'_{\lambda,2}$  will approximately be  $16 \mu\text{H}$  each.

**2. The B-field:** Assuming a magnetizing current  $I=100 \text{ A}$  (top value) equation (4.1) will give the flux density  $B_{d100} = 0.015 \text{ T}$ . (Two dimensional FEM-calculations  $0.0165 \text{ T}$ .) This is rather low for core materials as ferrites. This means that the sizing of the transformer is more governed by leakage flux and the ability to work even if the bus is misaligned to the fixed core part. Leakage flux has to be low, otherwise the voltage over the leakage inductance will limit the transformer power. Another thing that needs to be considered is that a misalignment lowers the coupling and also alters the resonant circuit in a way that lowers the possible power transfer, see section 2.1.1!

The misalignment and the distance the bus can be misaligned is related to the overall dimensions of the transformer and the air gap. With the data below in the table, it is assumed that the misalignment can be almost  $1 \text{ dm}$  in the bus moving directions and some centimetres in the orthogonal direction.

**3. Power losses in the core:** The flux density in the back iron core is:

$$B_c = \frac{\Psi/N}{2h_c l_c}$$

And the power losses related to this flux density in the iron core is:

$$P_c = 400B_c^2 m_c$$

[7], where  $m_c$  is the weight of the core material.

**4. Power losses in the windings:** The losses in the winding is partly ohmic losses,  $P_{cu} = RI^2$ , where  $I$  is the rms-value. The resistance  $R = \rho_{cu} L_{wind} / A_{cu}$  and in this case the total length of the primary winding  $L_{wind} = 11.2 \text{ m}$ .

As mentioned, the flux density in some transformer parts are low so there should not be any problem with losses in the core material. The power losses in the back iron can of course be high if the core is thin. The leakage flux that is developed when the transformer is loaded will however be a problem. See Figure 4.2.

The leakage flux will induce eddy currents in the windings if the conductor dimensions are higher than the skin depth. Compare with chapter 3, where equivalent resistance has been calculated!

The power losses due to eddy currents in the windings may be approximated as:

$$P_{hf} = V_{cu} \frac{(\omega d_{cu} B_x)^2}{32\rho_{cu}},$$

where  $V_{Cu}$  is the copper volume, [8].

The flux density is around  $B_x=0.02 \text{ T}$  and the frequency is high so the overall diameter of the conductor  $d_{cu}$  should be less than  $0.3 \text{ mm}$  in order to have a reasonable power loss due to the eddy current. The value calculated in Table 4.1 is calculated under the assumption of a diameter of  $0.3 \text{ mm}$  and  $B_x=0.02 \text{ T}$ . As shown in Figure 4.2 a lot of flux passes the winding in the case of a loaded transformer. This is partly due to the large air gap. How this shall be solved is just partly handled in this report and the calculated value is an approximative value.

Table 4.1: Transformer data

Transformer width	0.4 m
Transformer length	0.7 m
Core length, $\ell_c$	0.4 m
Centre core, $a_c$	0.1 m
Number of turns $N_1 = N_2$	7
Winding width $a_w$	0.1 m
Winding thickness, $h_l$	30 mm
Air gap	30 mm
'Tooth' length	35 mm
Thickness of core, $h_c$	15 mm
Conductor area*	105 mm <sup>2</sup>
Copper weight	13.2 kg
Core weight	94 kg
$L_m$	42 $\mu$ H
R 20 degC	1.1 m $\Omega$
Core losses	54 W
Total copper losses in the transformer	291 W @ 364 A**
Eddy current losses	2370 W

\* Fill factor of copper 35 %, stranded conductors with diameter 0.3 mm

\*\*See later in this chapter

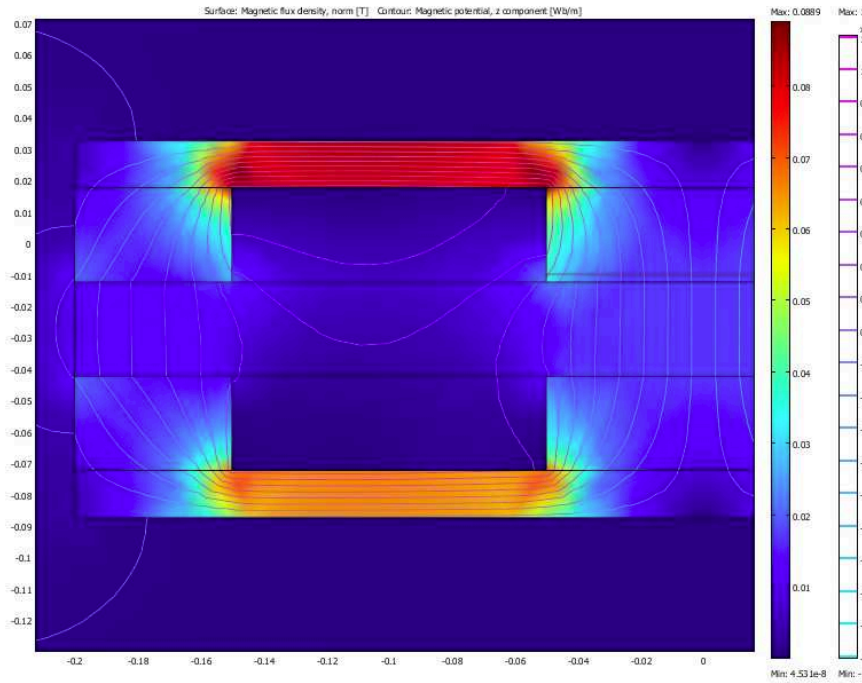


Figure 4.7: Transformer yoke, flux density and magnetic vector potential. Unloaded transformer.



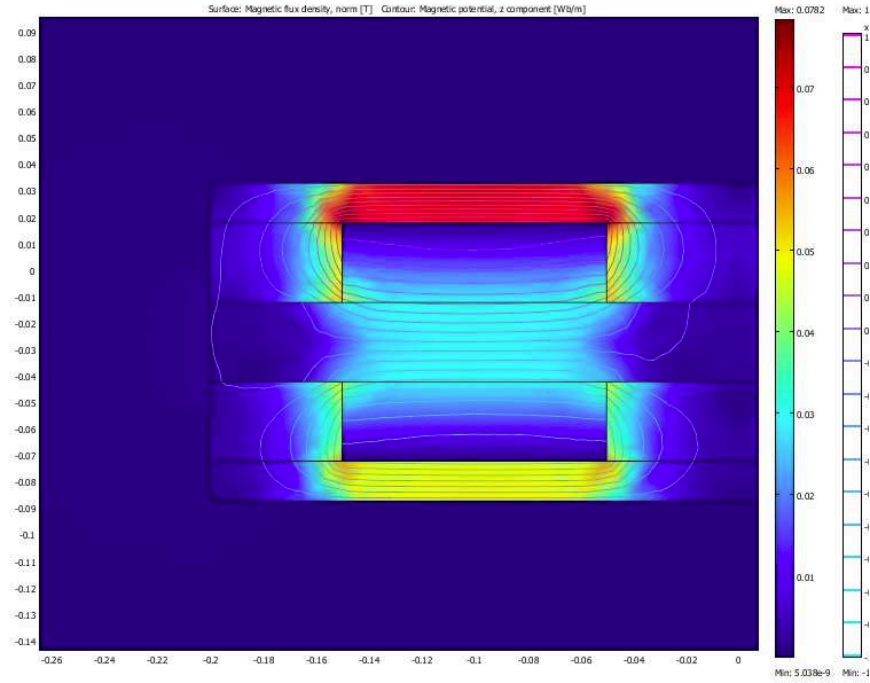


Figure 4.8: Flux density and magnetic vector potential in a loaded transformer. Active primary current = 350 A.

Further on in the calculations the transformer is handled as a lumped parameter circuit, according to Figure 4.9. The secondary current is transformed to the primary side using the transformer ratio:

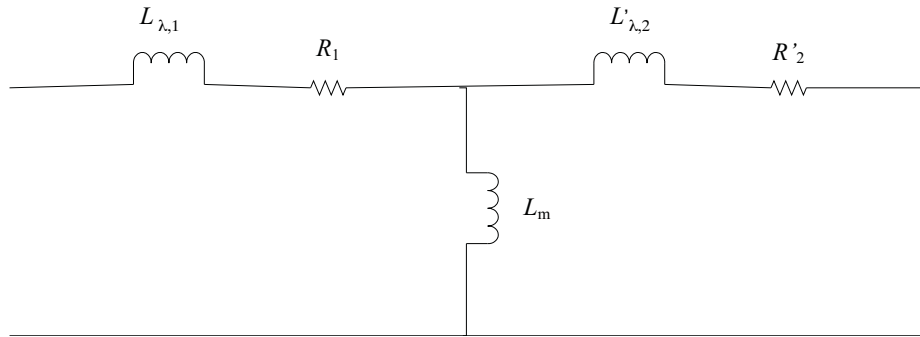


Figure 4.9: Approximation of inductive parts in the transformer.

### 4.3 Power Electronics

For the time being IGBT:s are probably the best choice for controlling the current to the transformer.

The power losses of the power IGBT:s are approximated from data sheets as function of current, voltage and switching frequency. The switching losses are represented by a second order polynomial and the coefficients are found through the Matlab function 'polyfit', producing the coefficients  $a_0$ ,  $a_1$  and  $a_2$ . The circuit is simulated and at every switching event it is decided whether or not it is an On-event, is there a diode involved or if it is an Off-event. One IGBT-module from Semikron and one from Infineon are compared.

$$E_{on} = a_0 + a_1 i + a_2 i^2$$

The conduction losses are,

$$p(t)_{cond} = U_{t0}i(t) + r_t i(t)^2$$

and the value is integrated over the simulation interval. The integrated value is divided by the simulation time and the latter is chosen as an integer number of the fundamental period time.

Table 4.2: Data of different IGBT-components

Parameter	SKM200GB123D/Semikron	FF200R12KS/Infineon
$U_{t0}$	1.5 V	1.7 V
$r_t$	10.7 m $\Omega$	7.2 m $\Omega$
$U_{d0}$	1.0 V	1.3 V
$r_d$	5.7 m $\Omega$	2.9 m $\Omega$
Eon/On-switch energy /mJ	$a_0=3.26, a_1=0.058, a_2 = 0.5e-3$	$a_0=5.57, a_1 = 0.016, a_2=0.3e-3$
Eoff /Off-switch energy /mJ	$a_0=3.39, a_1=0.078, a_2=0.1e-3$	$a_0=0.17, a_1=0.044, a_2= 0.1e-3$
Err/reverse recovery /mJ	$a_0=-0.14, a_1= 0.078, a_2= 0.2e-3$	$a_0=2.01, a_1= 0.063, a_2= 0.1e-3$

The power losses are summarized, in a case where the switching frequency is 25 kHz, see Figures 4.10 and 4.11. The switching losses of the component are high and the losses increase for currents that are not in phase with voltage. I.e. it is of several reasons interesting to have high power factor of the circuit.

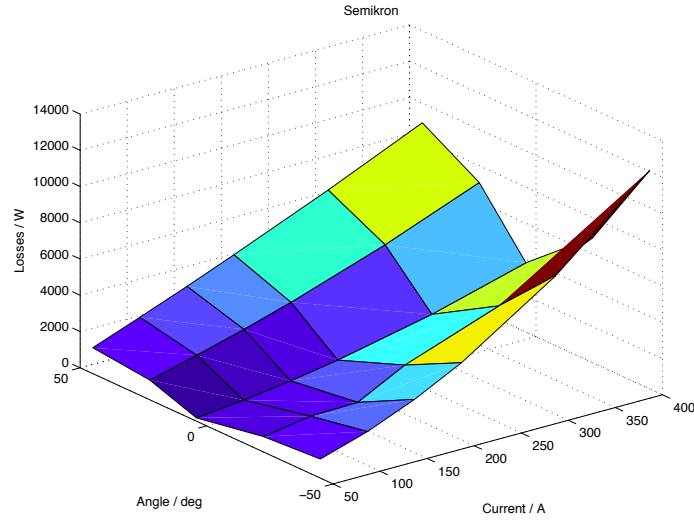


Figure 4.10: Power losses vs. current amplitude for Semikron

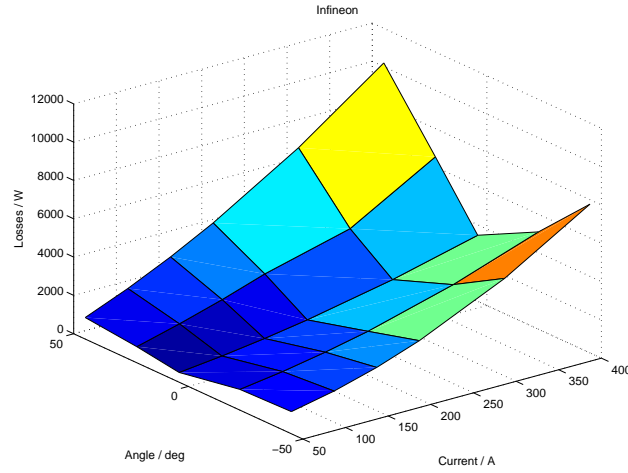


Figure 4.11: Power losses vs. current amplitude for Infineon

In this way, the voltage and current may be analyzed together with the passive components and in the same simulation the actual power losses are evaluated. At this relatively high switching frequency the losses associated with switching are the dominating part and it is of interest to keep this as low as possible. The way to lower the switching losses is to have low phase angle between the voltage and the current, which is beneficial for other reasons.

The power losses in the Infineon component is lower so it is used further on in the report.

## 4.4 Resonant circuit

As mentioned before, the resonant circuit will have a series capacitor in the primary circuit and a parallel circuit in the secondary circuit.

The transfer function is the output voltage divided by input voltage to the circuit:

$$H = \frac{U_2}{U_1}$$

$U_1$ : Input voltage,  $U_2$ : Output voltage

The transfer function from the primary voltage to the secondary side is shown in Figure 4.12.

According to [5] the resonant circuits should be tuned to the feeding frequency. Which in this case means

$C_{\text{prim}} = 3.53 \mu\text{F}$  in series to the inverter

$C_{\text{sec}} = 3.53 \mu\text{F}$  in parallel to the rectifier bridge:

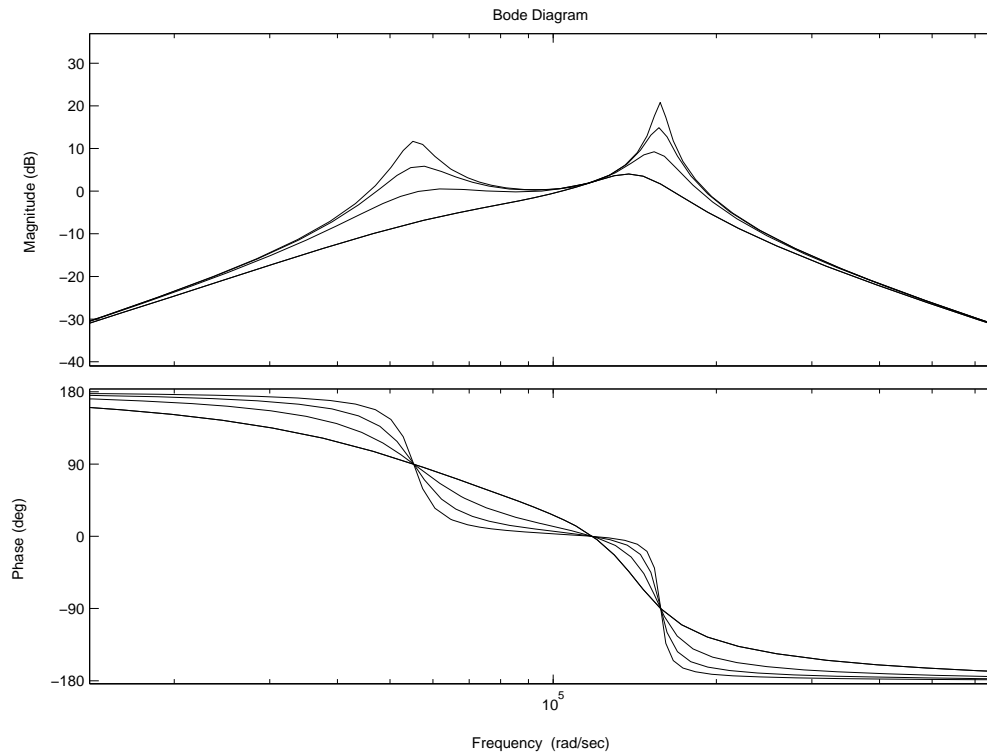


Figure 4.12: Bode analysis of transfer function H. Load resistance 2.2, 5, 10, 20  $\Omega$

## 4.5 Control of transformer current

One way to control the converter is to measure the current and wait for the zero-crossing and then switch the transistors. In this way the frequency will vary but low switching-losses are achieved over the range of load variations. Figure 4.13 shows current and voltage when this control strategy is applied in a fictive circuit, it works well but it has to be fine-tuned with appropriate circuit parameters.

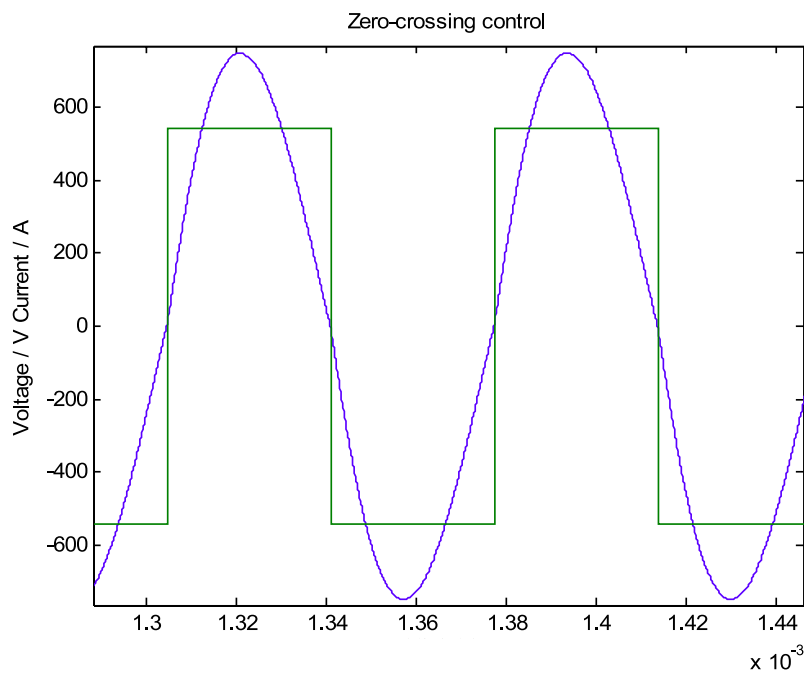


Figure 4.13: Converter output at current control.

Another way to avoid switching losses is to add a capacitor across every IGBT and always control it in inductive region. I.e. the current is always lagging the voltage with a small angle. In this case the frequency has to be chosen in such a way that we always have a current that is lagging the voltage.

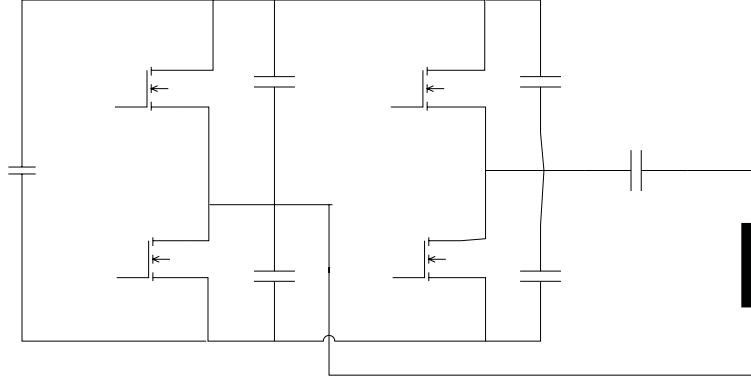


Figure 4.14: IGBT-converter with extra capacitors.

## 4.6 Model and simulation results

A Simulink model of the converter is implemented according to Figure 4.1. The model takes into account the switch-energy, but in our case we have assumed a converter with no or very low switching losses.

A power transfer of 112 kW is achieved when the loading resistance is  $1.5 \Omega$ , the primary voltage and current are shown in Figure 4.15. As can be seen in the figure, the current is almost sinusoidal although the voltage is a square wave. There is a phase lag between voltage and current, which should be minimized in order to optimize the size of the converter. The voltage and the power losses in one of the IGBT:s are also shown in Figure 4.6.

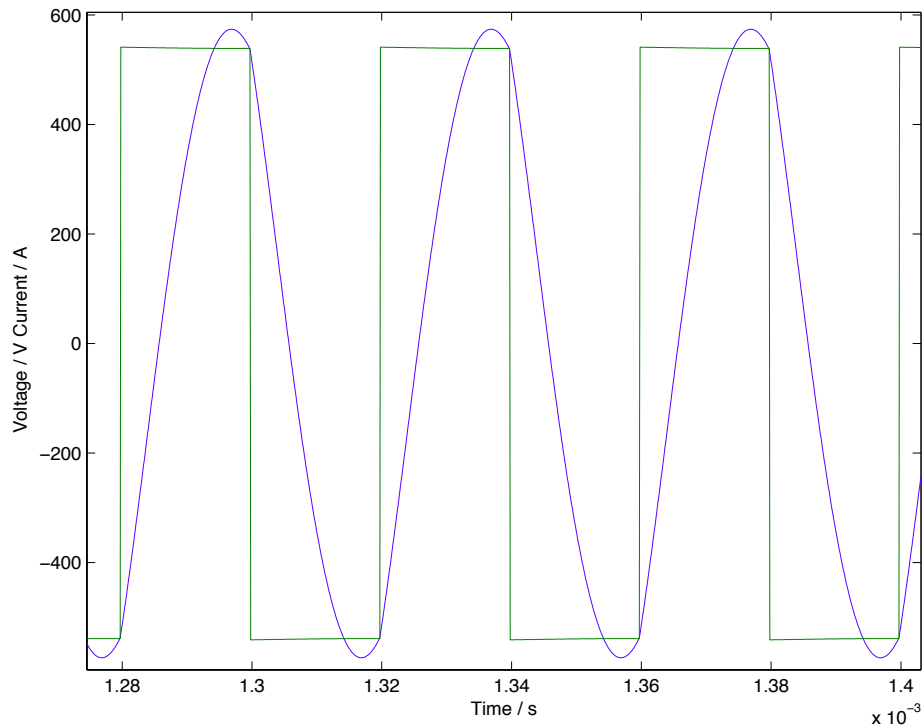


Figure 4.15: Voltage and current at 112 kW input power to the transformer.

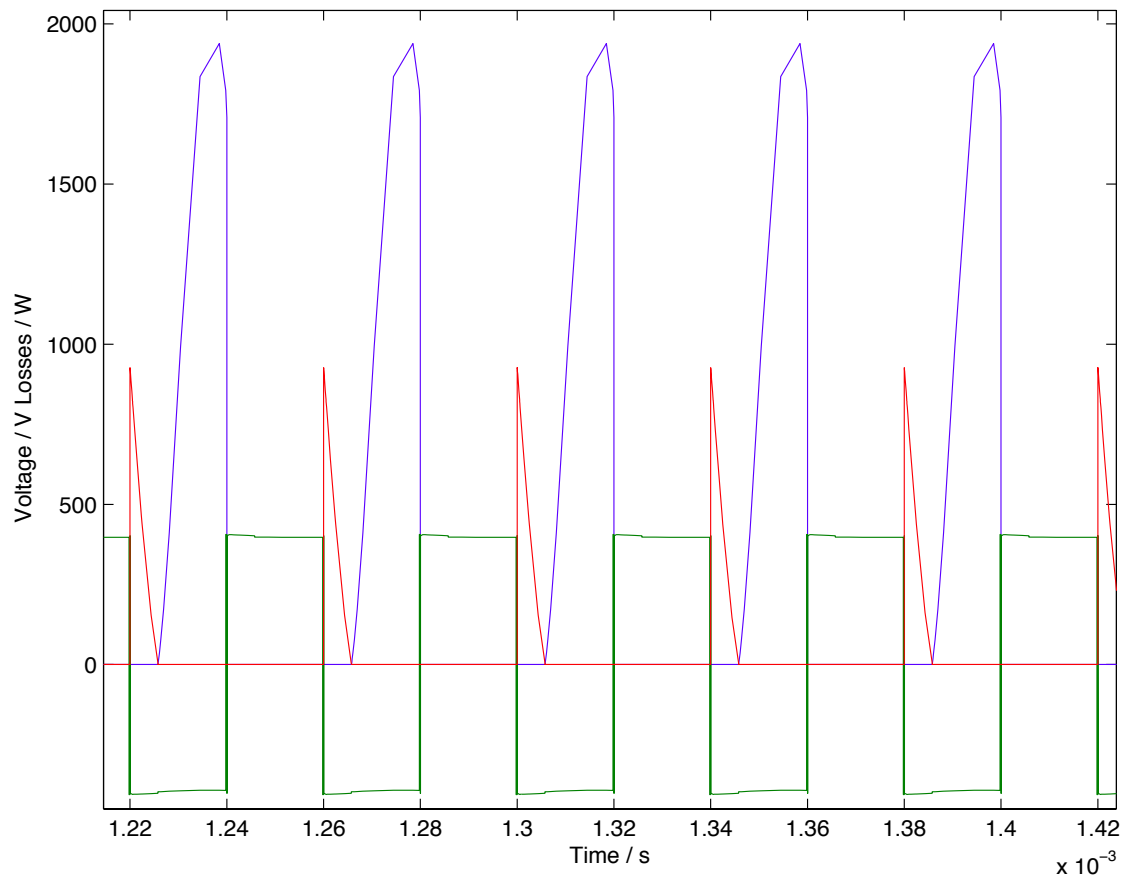


Figure 4.16: Voltage (green), conduction losses in the IGBT (blue) and conduction losses in the diode (red).

In this case, where we have in practice no switching losses, the losses of the inverter are shown in Table 4.3.

Table 4.3: Power losses in the converters

Infineon FF200R12KS	1860 W
Diode related (inverter)	230 W
Grid rectifier*	1500 W
Secondary rectifier**	2090 W
Total	5680 W

\* Assumed grid diode rectifier

\*\* Secondary rectifier of the same type as the primary inverter

The rectifying converter on the secondary side may be a simple diode rectifier or something more sophisticated as a controlled H-bridge. In the case of a rectifier, the primary current and voltage are shown in Figure 4.17 and in Figure 4.18 the rectifier current.

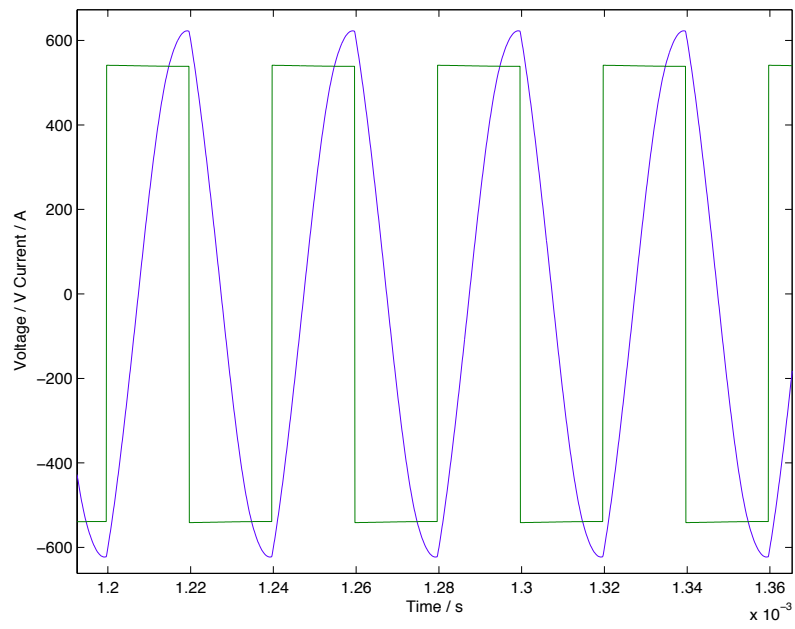


Figure 4.17: Primary voltage and current

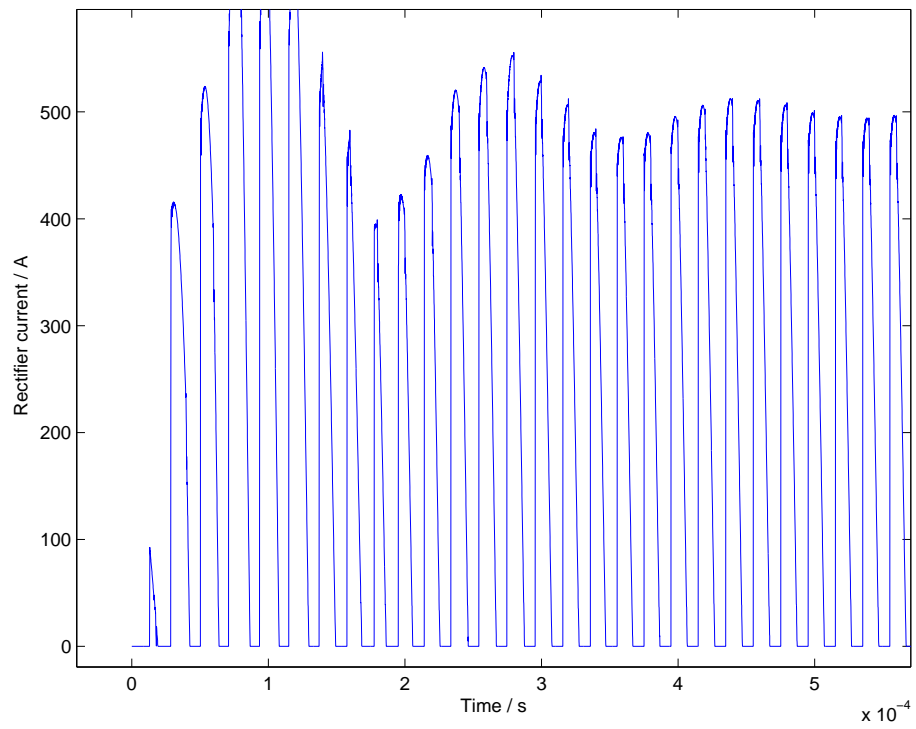


Figure 4.18: Rectifier current.

The circuit filters the rectifier current in an efficient way.

The losses in the primary and secondary winding is 383 W, core losses are estimated to 54 W. The magnetizing current according to Figure 4.19 have a relatively high amount of harmonic components. This should be addressed in future work. Eddy currents in the winding are very much depending on how the winding is done and this has to be studied more in detail. The first result indicates a 10 % loss compared to the transmitted power and it should be addressed in some way. Either avoiding flux through the winding which might be difficult or using thinner conductors.

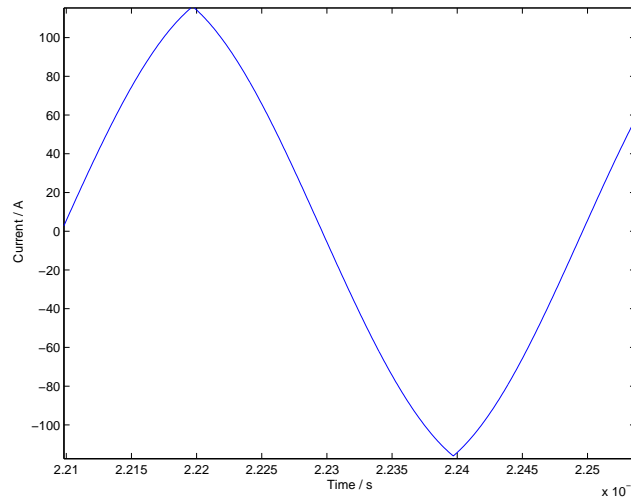


Figure 4.19: Magnetizing current,  $I_m$ .

The calculated copper losses, except for eddy current losses, will increase when the winding heats up but the losses in the transformer are still below 1 % of the transmitted power so it is a low value and a matter for further studies. Taking into account the losses in the power electronics, the overall efficiency is  $> 94\%$ . If we take into account the eddy current losses the efficiency is below 90 %. It is based on some simplified assumptions and a more thorough calculation of the losses is necessary.

## 4.7 Alternative system

An alternative to this system is to use some sort of system that aligns the transformer halves and also adjust them together. If for instance the air gap is decreased to 3 mm, the transformer size may be halved and still will the inductance be increased to  $l = 12\mu\text{H/m}$ .

The leakage flux will be lowered to only five percent and there is no need for resonant circuits. The charging current may be controlled by the primary circuit and everything in the electric circuit will be simpler, cheaper and smaller.

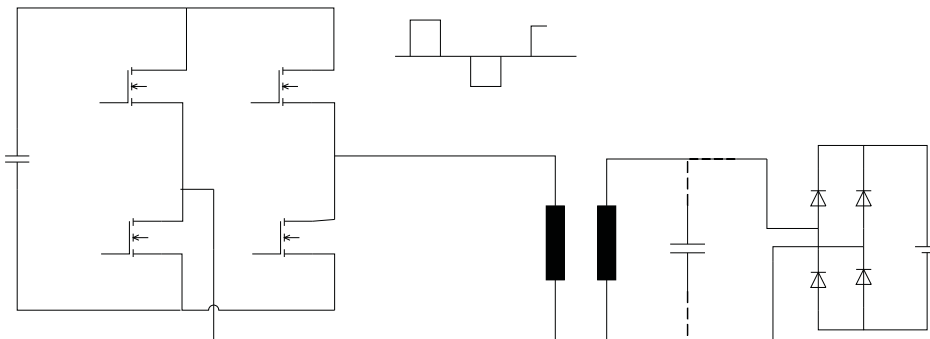


Figure 4.20: Alternative system



The data of the transformer is according to Table 4.4 and the size is much lower. The resistance is almost the same with one quarter of the copper mass. Of course there will be higher loss density both in the winding and in the core so the thermal aspects must be investigated but it might still be a good alternative. The high frequency eddy current losses are very much lower in this transformer type which may be a good reason for investigating this alternative properly.

Table 4.4: Alternative transformer data

Transformer width	0.15 m
Transformer length	0.21 m
Centre core, $a_c$	0.038
Number of turns $N_1 = N_2$	7
Winding width 30% , $a_w$	0.038 m
Winding thickness, $h_l$	30 mm
Air gap	30 mm
'Tooth' length	35 mm
Thickness of core, $h_c$	30 mm
Conductor area	56 mm <sup>2</sup>
Copper weight	3 kg
Core weight	14.7 kg
$L_m$	38 $\mu$ H
R 20 degC	0.91 m $\Omega$
Core losses	74 W
Copper losses	241 W @ 364 A
Eddy current losses	1037 W

The Simulink model is changed, so that the converter is directly coupled to the primary coil of the transformer and the secondary coil is connected to the rectifier. A small capacitor, 1  $\mu$ F, is in parallel to the rectifier and the simulated voltage and current are shown in Figure 4.21. The resulting data of the circuit are highlighted in Table 4.5.

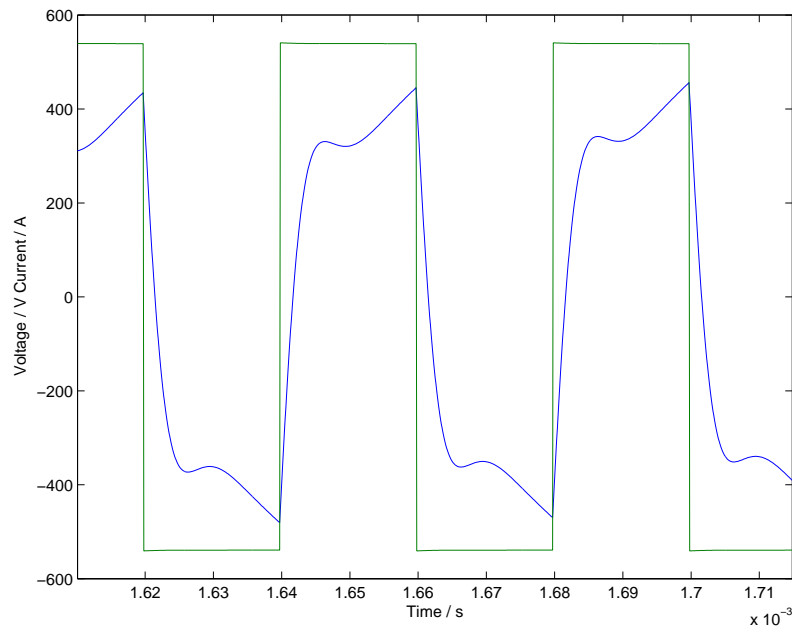


Figure 4.21: Voltage and current to a transformer with small air gap

Table 4.5: Power losses in the converters, alternative solution

Infinion FF200R12KS	1860 W
Diode related (inverter)	230 W
Grid rectifier*	1500 W
Secondary rectifier**	1500 W
Total	5090 W

\* Assumed grid diode rectifier

\*\* Secondary rectifier of the same type as the primary inverter

This alternative has the potential of having an efficiency of 93-94 %.

Another alternative is extreme frequency, 10 MHz, which is used on in [6] where reflecting metallic planes are used for creating an electromagnetic resonance that makes it possible to transmit power over a distance of 2 m. We are talking on antennas which is a complete other business but it is claimed to have an efficiency of 97 % in the transmission part. In order to analyze this, other calculation tools should be used and we also need components that can operate at 10 MHz with high power loading.

## 4.8 Conclusions of Chapter 4

The relatively long air gap of the 'transformer' has some implications. There will be high leakage. A lot of flux will penetrate the winding. The amount of copper that is exposed to high frequency flux will have high losses, if the conductors are not thin.

The leakage flux must be controlled so that the flux density levels in the vicinity of passengers will be below acceptable levels.

The overall losses of the conversion is very much depending on the winding construction, so special care must be taken. Probably the winding has to be made by Litz-wire.

A comparison with a transformer with a low air gap indicates higher efficiency and almost one-seventh of the active material. Some simplifications can be made also to the converter and control. A system that locates and controls the position of the transformer halves must be added in this case.

Finally the efficiency of a 100 kW charging system was investigated. It was found that the efficiency was approximately 94 %. However in a case with large air gap the winding construction is very important and in order to avoid high losses Litz-wire has to be used. The thin conductors of a Litz-wire makes it possible to lessen the eddy currents and skin effect in the conductors.

One possible solution is to use a system that locates the transformer halves to each other. In this case the material use drops dramatically.

## Chapter 5

### Conclusions

In this work the theory of wireless charging was developed. FEM analyses on both 2D and 3D models were performed using Maxwell and Comsol Multiphysics. Moreover, analytical methods were also developed and compared with the FEM results and some key results were compared with measurements.

The larger the air gap between a receiving and a sending coil, the less sensitivity to displacements, but also less mutual inductance. Less sensitivity can also be achieved if the coils of the receiving coil are placed next to each other. This is shown more effective than placing the coils as one inner ring coil inside an outer ring coil. It is also shown better than placing the receiving coils above each other.

Further, it is shown efficient to use ferrite plates adjacent to the coils. The plates need to be large in order to avoid high magnetic fields outside the charging system, as the maximum value of the magnetic field will occur just outside the ends of the ferrite plates.

It is also shown that if the coils (sending and/or receiving) have several conductors, then it is best to move the outer conductors away as this will reduce the skin effect, and therefore reduce the coil resistance.

Adding a resonant C to the secondary circuit will raise the transmitted power up to 400 times when using a resonant set-up.

Differently shaped coils may be modelled, and resistance and inductance values calculated. The mesh quality is shown important, especially for the calculation of the resistance at high frequencies. It is also important to compare the results with different solvers, measurements and if possible with analytical calculations.

Inductance and resistance of one and two ring coils were determined analytically with two solvers in Maxwell with very accurate results. When comparing with measurements the discrepancy was larger, which could be explained with the complicated helix coils, necessitating a simplified 3D model. Still both the resistance and inductance values were shown to be rather similar for FEM calculations and measurements. When comparing the results for a 25-coil system, the difference was small ( $<5\%$ ) regarding inductance, whereas the resistance values were more astray due to the difficulty to model the Litz-wire properly.

The relatively long air gap of the 'transformer' has some implications. There will be high leakage. A lot of flux will penetrate the winding. The amount of copper that is exposed to high frequency flux will have high losses, if the conductors are not thin. The leakage flux must be controlled so that the flux density levels in the vicinity of passengers will be below acceptable levels.

Finally the efficiency of a 100 kW charging system was investigated. It was found that the efficiency was approximately 94 %. However in a case with a large air gap, the winding construction is very important and in order to avoid high losses Litz-wire has to be used. The thin conductors of a Litz-wire makes it possible to lessen the eddy currents and skin effect in the conductors. One possible solution is to use a system that locates the transformer halves to each other. In this case the material use drops dramatically.



# Bibliography

- [1] Eva Palmberg, Lecture notes in Electromagnetic Design Course, Chalmers 2012
- [2] Eva Palmberg 2012, "Electromagnetics Revised" Course Compendium at the division of Electric Power Engineering, the department of Energy and Environment at Chalmers University of Technology, Göteborg, Sweden 2012.
- [3] Mikael Cederlöf (2012) "Inductive Charging of Electrical Vehicles", Master Thesis at KTH Electrical Engineering, Stockholm, Sweden 2012.
- [4] Björkman Jimmy, Ekman Christian, Gustavsson Erik, Hagman Niklas, Hansson Gustav, and Majdandzic Davor (2012) "Trådlös multifrekvensladdare för el-gocart", Bachelor Thesis at the division of Electric Power Engineering, the department of Energy and Environment at Chalmers University of Technology, Göteborg, Sweden 2012.
- [5] Wang, Stielau, Covic "Design Considerations for a Contactless Electric Vehicle Battery Charger", IEEE Transactions on Industrial Electronics, vol.52 No.5 Oct-05
- [6] Xiaofang Yu, Sunil Sandhu, Sven Beiker, Richard Sassoon and Shannui Fan "Wireless energy transfer with the presence of metallic planes", Appl.Phys. Lett. 99, 214102 (2011); doi: 10.1063/1.3663576
- [7] Data sheet from EPCOS u<sub>141\_78\_30</sub>.pdf
- [8] Charles R. Sullivan, Member IEEE, Computationally Efficient Winding Loss Calculation with Multiple Windings, Arbitrary Waveforms and Two-Dimensional or Three-Dimensional Field Geometry, IEEE Transactions on Power Electronics, vol. 16, No 1, January 2001